Investigation of Aircraft Noise Metrics

Analysis of Certification and Community Noise Metrics

T. Van Hemelen

TU Delft

Investigation of Aircraft Noise Metrics

Analysis of Certification and Community Noise Metrics

by

T. Van Hemelen

to obtain the degree of Master of Science
at the Delft University of Technology,
to be defended publicly on Tuesday April 25^{th}, 2017 at 11:00 AM.

Student number:	4168534	
Project duration:	February 1, 2016 – March 1, 2017	
Thesis committee:	Prof. Dr. D.G. Simons,	TU Delft
	Dr. Ir. A. Sahai,	TU Delft, supervisor
	Dr. Ir. R. Vos,	TU Delft
	Dr. Ir. M.I. Gerritsma,	TU Delft

An electronic version of this thesis is available at `http://repository.tudelft.nl/`.

TU Delft

Preface

> Scientists discover the world that exists;
> engineers create the world that never was.
>
> Theodore von Karman

Nearly two years ago, I accepted an internship offer at The Airbus Future Projects Office, in Toulouse, simply named *Acoustic Value*. During six months I worked on the financial quantification of aircraft noise, a project which sparked my interest in aircraft noise. Near the end of my internship I was faced with a challenging problem I could not tackle with the time I had left. Unwilling to give up, I contacted professor Simons and proposed this problem as my thesis topic.

Professor Simons brought me in contact with my thesis supervisor Dr. Abhishek Sahai. Together we discussed the topic and saw an opportunity to kill two birds with one stone. On my part I required aircraft noise simulations, to formulate and prove an hypothesis, while Dr. Sahai required someone to bring together a noise simulation framework. This framework would be composed out of programs available within the department of Flight Performance & Propulsion and the department of Aircraft Noise & Climate Effects. What I liked most about this combination was that it allowed me to work on different disciplines at once and see how they came together. As a result, during this thesis I have gained knowledge and experience in aircraft design, aero engines, flight performance, and aircraft noise.

As always with large projects, some parts went really well, while others proved to be a bit more challenging. Since this thesis was a rollercoaster ride of ups and downs it taught me many great things on project managing and myself. Most importantly, it taught me that you are never alone in your endeavours. Therefore, I would like to express my gratitude to those who accompanied me on this journey. First of all I would like to thank Dr. Abhishek Sahai for his supervision and council during this project. Furthermore, I would like to thank Dr. Feijia Yin and Dr. Roelof Vos for their advice on engine and aircraft design programs. Special thanks goes out to Paul Dermarkar, Nadine Genoulaz, and Anne Dumoulin from Airbus, who had a keen interest in my work throughout the entire duration of this project and provided me with valuable insight and suggestions.

Technical advice was not the only support I received. There are many friends and family members I should thank for lifting my spirit in time of need and helping me find balance between thesis and myself. Foremost, I thank Christina, my girlfriend and major support throughout this project. My parents deserve a special place as well,for their support throughout my studies.

During my studies in aerospace engineering I have learnt a great deal about myself and the world around me. This thesis is the grand finale of my studies and allowed me to create a small part of the world that never was. With my studies concluded I'm at the doorstep of my future career and the world of tomorrow.

Tom Van Hemelen
Delft, February 2017

Summary

As awareness for aircraft noise increases, local authorities and airports try to manage the problem by implementing a range of noise abatement measures. Often aircraft operators will face operational restrictions and noise charges. For this a quantification of aircraft noise is required. The Effective Perceived Noise Level or EPNL is the industry's standard for quantifying aircraft noise. Local environmental legislation, however, mostly makes use of the A-weighted sound pressure level, L_A. The problem is that EPNL and L_A are fundamentally different and no straight forward conversion exists from one to the other. During conceptual aircraft design, the certification noise level is often known as a target, while the community noise level L_A remains undefined. Therefore to properly assess the community noise impact during conceptual design, a relationship is needed linking the certification noise level to the L_A level. Besides L_A, the Sound Exposure Level (SEL) was also investigated.

To find the relationship between EPNL, L_A, and SEL, aircraft noise simulations were required. For this purpose the aircraft noise simulation framework was created by linking simulation software available within the Flight Performance & Propulsion department and the Aircraft Noise & Climate Effects department of the Faculty of Aerospace Engineering at TUDelft. The result is a method in which the Intiator program was used to design an aircraft, which was powered by an engine modelled in GSP and flown by a point mass trajectory model. Based on this, the aircraft noise was then estimated using the INSTANT noise prediction program. Five aircraft were selected for the analysis: the A320, A330, Fokker 100, long range aircraft 1, and long range aircraft 2. The Initiator was used to recreate these aircraft, and together with the reference aircraft, this led to a total of ten aircraft. With their engines modelled in GSP, these aircraft were subjected to ICAO's noise abatement departure procedure 1 and the standard ICAO approach for the calculation of their trajectories. The results were processed by INSTANT to provide a prediction of the aircraft noise with three outputs. The first output was the EPNL certification level at the three certification points, the second was the departure and approach noise contours in the three metrics.

These reference aircraft were validated by comparing them to their real life counterparts, using the EASA noise certificate database and examples in literature. For take-off and approach, it was seen that the predicted aircraft noise certification values estimated were higher than those observed in reality, while the estimated sideline noise was lower. The reason for this is that the flight procedures used resulted in flight trajectories lower than the heavily optimised trajectories used during certification. As a result the emitted noise experiences less geometric spreading and atmospheric absorption, largely explaining the deviation. The predicted noise contours were seen to be realistic in both magnitude and shape. The deviations in the noise simulations do not affect the analysis of the metrics, as the relationship is independent from the magnitude of the noise. For the analysis of the metrics relationships both reference and Initiator aircraft were used. Correlating the EPNL level at the certification points to the areas contained within the noise contour showed a strong relationship between the three metrics. The next step was correlating the areas within the contours of the metrics to each other, which confirmed the existence of a relationship on contour level. An artificial neural network was then successfully used to define a relationship between EPNL, L_A, and SEL based on the certification noise level of the aircraft, parameters describing the size of the aircraft, and parameters describing the engine. The neural network was successful in estimating the acoustic performance of aircraft which are close to the learning dataset of the neural network. Significantly larger or smaller aircraft led to less accurate predictions. The neural networks for departure and approach are stored in a MATLAB function, which operates with very little computational effort. Therefore this relationship can easily be used in programs such as Initiator.

The relationship is based on data of conventional aircraft with two wing mounted (two spool) turbofan engines. Therefore the relationship is limited to these aircraft. However, most modern civil airliners fall under this definition. Taking these limitations into account, the relationship can estimate aircraft noise during the conceptual design stage with very limited input and computational effort, achieving the goal of this thesis project.

Contents

List of Figures

List of Tables

Acronyms

2D	2 Dimensional
3D	3 Dimensional
AM	Adaptive Modelling
ANCE	Aircraft Noise & Climate Effects
AVL	Athena Vortex Lattice
BPF	Blade Passage Frequency
CROR	Counter Rotating Open Rotor
DP	Design Point
EASA	European Aviation Safety Agency
EOM	Equations of Motion
EPNL	Effective Perceived Noise Level
EPR	Engine Pressure Ratio
FAA	Federal Aviation Authority
FF	Fuel Flow
FPP	Flight Performance & Propulsion
GSP	Gas Turbine Simulation Program
HP	High pressure
ICAO	International Commercial Aviation Organisation
IFD	Inlet Flow distortion
IGVs	Inlet Guide Vanes
INSTANT	ILR Noise Simulation and Assesment module
ISA	International Standard Atmosphere
JFK	John F. Kennedy airport (New York)
KPI	Key Performance Indicator
LP	Low pressure
LR	Long Range
MDO	Multi-Disciplinary Optimization
MTOW	Maximum Take-Off Weight
NADP	Noise Abatement Departure Procedure
NASA	National Aeronautics and Space Administration
NDE	Non-linear Differential Equations
NLR	National Aerospace Laboratory
OD	Off-Design
OEW	Operative Empty Weight
PMM	Point Mass Model
PNL	Perceived Noise Level
PNLT	Tone-Corrected Perceived Noise Level
SPL	Sound Pressure Level
TIT	Turbine Inlet Temperature
TLRs	Top Level Requirements
TUDelft	Delft University of Technology
XML	Extensible Markup Language

List of Symbols

A	Wing aspect ratio
$A_{combustor}$	Combustor entrance area
A_f	Flap area
A_{fan}	Fan inlet area
A_h	Horizontal tailplane area
A_{in}	Entrance area
A_{inlet}	Inlet area
$A_{j,1}$	Primary jet area
$A_{j,2}$	Secondary jet area
A_{out}	Exit area
A_{throat}	Exhaust throat area
$A_{turbine}$	Turbine inlet area
A_v	Vertical tailplane area
A_w	Wing area
a or a_i	Empirical power coefficient
B	Number of rotor blades
$B_{turbine}$	Number of turbine blades
BPF	Blade Passage Frequency
b	Empirical power coefficient
b_f	Flap span
b_h	Horizontal tailplane span
b_v	Vertical tailplane span
b_w	Wing span
C	Tone correction factor
C	Coherence coefficient
c_∞	Free stream speed of sound
D	Duration correction
D or D_m	Directivity function
D	Drag force
D_g	Drag force due to groundfriction
d	Fan rotor diameter
$d_{landing}$	Landing distance
d_{MG}	Main landing gear wheel diameter
d_{NG}	Nose landing gear wheel diameter
d_p	Plug diameter
d_{TKO}	Take-off distance
$d_{turbine}$	Turbine rotor diameter
dp_{comb}	Design point relative pressure losses
$EPNL$	Effective Perceived Noise Level
$EPNL_{APP}$	Approach Effective Perceived Noise Level
$EPNL_{certif}$	Effective Perceived Noise Level for certification
$EPNL_{LAT}$	Lateral Effective Perceived Noise Level
$EPNL_{TKO}$	Take-Off/Flyover Effective Perceived Noise Level
EPR	Maximum engine pressure ratio

F	Difference original and background SPL
F or F_m	Spectral function
FAR	Fuel to air ratio
FN	Net thrust
f	Frequency
G	Attenuation factor
G_c	Coaxial nozzle correction
G_i	Geometry effect factor
$G_{i,j}$	Factor for IGV and tone cut-off
G_p	Plug nozzle correction
H_{cr}	Cruise altitude
H_{fe}	Runway field elevation
H_{fl}	Flare altitude
H_{igs}	Glideslope interception altitude
H_{level}	Level approach flight altitude
H_{lo}	Height lift-off above runway
H_m	Correction for forward flight effect
H_S	Screen height
h	Altitude observer
h	Specific enthalpy
h_a	Aircraft altitude
h_o	Altitude observer
h_r	Relative humidity
I	Moment of inertia
K or K_i	Empirical constant
k	Wave number
L	Lift force
L_A	A-weighted Sound Pressure Level
L	Characteristic length
l_{MG}	Main landing gear strut length
l_{NG}	Nose landing gear strut length
M_{cr}	Cruise Mach number
$M_{j,1}$	Primary jet Mach number
$M_{j,2}$	Secondary jet Mach number
M_m	Design Mach number
M_r	Blade tip Mach number
$M_{t,d}$	Fan rotor tip Mach number at design point
M_v	Mass in a volume v
M_x	Axial flow Mach number
M_∞	Free stream Mach number
m	Mass of aircraft
m_{fuel}	Fuel mass
$m_{payload}$	Payload mass
$\dot{m}$	Fan mass flow rate
$\dot{m}_{combustor}$	Combustor mass flow rate
$\dot{m}_{des}$	Design mass flow
$\dot{m}_f$	Fuel flow
$\dot{m}_{in}$	Ingoing mass flow
N	Overall Noy value
N	Low pressure spool rotation speed
N	Net force
N_{des}	Design spool speed
n	Number of segments
n_{cycles}	Number of flight cycles
$n_{engines}$	Number of engines
n_i	Noy value of the i^{th} spectrum band

n_{max}	Maximum Noy value
n_{pax}	Number of passengers
PNL	Perceived Noise Level
$PNLT$	Tone-Corrected Perceived Noise Level
$PNLT_{max}$	Maximum Tone-Corrected Perceived Noise Level
PR	Pressure ratio
r_{ref}	Reference pressure
PW_{abs}	Power
p	Pressure
$p_{t,i}$	Combustor entrance total pressure
$p_{t,j}$	Combustor exit total pressure
$< p^2_{i,j} >$	Mean-square pressure of source i for component j
$< p^2(l_{ref}, 90°) >$	Mean-square pressure at reference length l_{ref}
Q	Heat flux
R	Wave magnitude
R	Specific gas constant
R_{cr}	Cruise range
R_{div}	Divergence range
r	Radius
r_s	Source radius
S	Spectral function
SOT	Stator outlet temperature
SPL	Sound Pressure Level
SPL'	Adjusted sound pressure level
SPL''	Adjusted SPL'
s	Change in SPL
s'	Adjusted change in SPL
$\bar{s}$	Average of adjacent s'
s/c	Rotor-stator spacing
T	Temperature
T	Thrust
T_{exit}	Turbine exit temperature
T_g	Gas temperature
T_j	Turbine exit static temperature
$T_{j,1}$	Primary jet temperature
$T_{j,2}$	Secondary jet temperature
$T_{t,i}$	Combustor entrance total temperature
$T_{t,i}$	Turbine entrance total temperature
$T_{t,j}$	Combustor exit total temperature
T_{01}	Reference temperature
t	Time
t_{lag}	Engine spool-up time
t_{loiter}	Loiter time
V	Number of stator vanes
V	Velocity of aircraft
V_{comp}	Component volume
V_R	Rotation speed
V_{stall}	Stall speed
$v_{j,1}$	Primary jet velocity
$v_{j,2}$	Secondary jet velocity
W	Weight of aircraft
W_{in}	Mass flow in
W_{out}	Mass flow out
$W_{payload}$	Payload weight
z	Altitude

α	Absorption coefficient
α	Angle of attack
α_T	Thrust angle of attack
γ	Elevation angle aircraft and observer
γ	Ratio of specific heats
γ	Flight path angle
γ_{gs}	Glideslope angle
Δs	Change in s
ΔT	Total temperature rise across fan
ΔT_{des}	Design point temperature extraction from turbine
δ	Engine inlet axis angle
δ_f	Flap deflection angle
δ_w	Dimensionless turbulent boundary layer thickness
η	Frequency parameter
η_{comb}	Combustion efficiency
$\eta_{fan_{bypass}}$	Bypass side fan efficiency
$\eta_{fan_{core}}$	Core side fan efficiency
$\eta_{gear_{fan}}$	Fan drive gearbox efficiency
$\eta_{HP_{comp}}$	HP compressor efficiency
$\eta_{HP_{turb}}$	HP turbine efficiency
$\eta_{LP_{comp}}$	LP compressor efficiency
$\eta_{LP_{turb}}$	LP turbine efficiency
$\eta_{mech_{HP_{turb}}}$	HP turbine mech. efficiency
$\eta_{mech_{LP_{turb}}}$	LP turbine mech. efficiency
θ	Polar angle
θ	Pitch angle
θ_{aim}	Rotation angle
μ_g	Runway friction coefficient
Π_w	Acoustic power function
ρ	Density
$\rho_{j,1}$	Primary jet density
$\rho_{j,2}$	Secondary jet density
ρ_∞	Free stream fluid density
σ	Specific effective flow resistivity
ϕ	Azimuth angle
ω	Angular velocity

1

Introduction

Aircraft noise nuisance has been a problem since the dawn of the jet age. With the introduction of passenger jet aircraft such as the Boeing 707 came the rolling thunderous noise and high pitch squeals of the jet engine. The astounding difference in noise between the, at the time, contemporary propeller and jet planes resulted in public uproar. Eventually even threatening the newborn jet aircraft with being banned from major airports such as New York's Idlewild, now JFK. This threat spurred research resulting in the development of the field of aeroacoustics, the Effective Perceived Noise Level (EPNL) metric, and the first noise abatement procedures [9]. Aviation has evolved drastically since the fifties and modern jet aircraft have become considerably more silent than their predecessors, as can be seen in Figure 1.1:

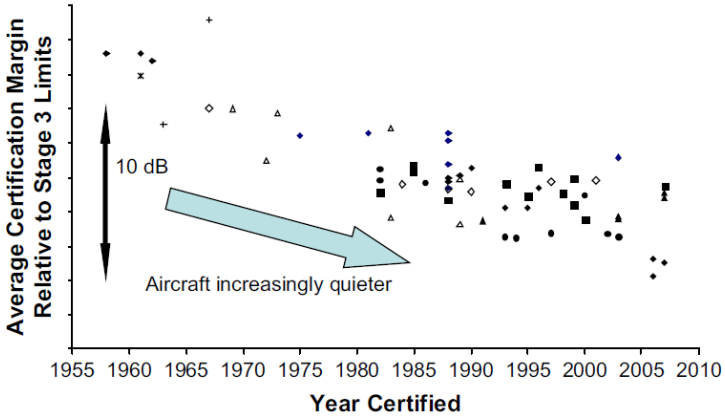

Figure 1.1: The evolution of aircraft noise [1]

While aircraft became more silent throughout the years, the number of aircraft movements increased, resulting in an elevated perception and awareness of aircraft noise. This led to local authorities and airports to introduce noise abatement measures in an effort to mitigate the effects of aircraft noise. These measures are often implemented as noise charges and operational restrictions, e.g. night bans, and can lead to major revenue reductions for aircraft operators [1, 10].
Environmental concerns for noise are not limited to aircraft but extend to all forms of industry and transportation ranging from discotheques to trains. Local authorities tend to regulate these noise emission with guidelines and laws. Therefore since noise is not limited to the aviation industry the more generic L_A or A-weighted decibel metric is sometimes used in these regulations instead of the aviation EPNL metric [11–14].

The advantage of the EPNL metric is that it gives the noise level of the aircraft during certification, under conditions which are nearly constant. Hence as a disadvantage it might not reflect the local conditions near an airport. The L_A metric is thus very dependent on local conditions such as climate, geography, and microphone placement [2]. During the early design stages of the aircraft the noise is quantified as a target described by the EPNL metric, however a conversion from EPNL to L_A would require hefty simulation tools with inputs

which might not be available during these stages of design[15]. This problem marks the need for a relatively simple prediction method which can relate the EPNL level of an aircraft to the community noise exposure expressed in L_A using basic aircraft parameters as input (e.g. thrust, span, fuselage length, and EPNL level). For completeness it was also decided to investigate the relationship of the two noise metrics to the Sound Exposure Level (SEL), which is a time-integrated measure of L_A.
To investigate the aircraft noise issue an aircraft noise simulation framework was developed using software readily available within the Flight Performance & Propulsion (FPP) and the Aircraft Noise & Climate Effects (ANCE) departments of the Faculty of Aerospace Engineering at Delft University of Technology. The development of this framework was an internal task within these departments. Investigating different aircraft designs within this framework helped to determine a correlation between EPNL, L_A, and SEL for different aircraft. A representation of the framework is shown in Figure 1.2, where an aircraft designer and engine simulator will deliver the aircraft and engine model to a flight trajectory simulator. This flight trajectory simulator will then simulate the aircraft in flight and transfer all necessary data to the noise simulator. Note that since aircraft noise is mostly limited to areas near airports, the work done during this project will consider only the take-off and approach stages of flight.

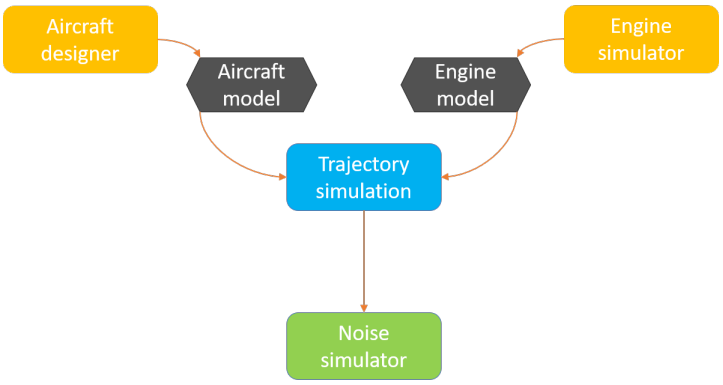

Figure 1.2: Desired noise prediction framework

This project attempts to fulfil two needs: one scientific, and one practical one within the ANCE and FPP departments. The scientific need is the determination of a relationship between EPNL, L_A, and SEL. To find this relationship the aircraft noise simulation framework was developed fulfilling the practical need as well in one go. In turn the framework will open up more possibilities for research in aviation acoustics, such as this project.

A clear definition of the scope of this project can be found in Chapter 2. When the scope is defined the reader will be introduced to the basics of noise metrics and aircraft noise modelling in Chapters 3 and 4, respectively. The methodology used in this project is laid out in Chapter 5, followed by the results in Chapter 6. The conclusion is provided in Chapter 7 along with several recommendations on improvements to the aircraft noise simulation framework and its use in future research.

2

Research Questions, Objective, and Scope

The research questions form the basis of the project, this chapter will provide all research questions applicable to this thesis project along with a clear definition of the objective(s) to be achieved. The research questions follow from the research aim and objective:

*The research aim of this project **is to** investigate the relationship between the EPNL noise level of a conventional aircraft to the L_A level **by** using an aircraft noise model to simulate aircraft flyovers for different aircraft.*

The answers to the research questions are pieces of a puzzle joining together in order to reach the research objective. The project research questions build up the knowledge required to solve the problem and are:

1. Can a relationship be found between aircraft noise expressed in EPNL and L_A for a given aircraft?
   (a) How can an aircraft noise simulation framework be made?
      i. How can the aircraft's noise emission be modelled?
      ii. How can the aircraft's engine be modelled?
      iii. How can the aircraft's flight trajectory be modelled?
      iv. How can different aircraft models be quickly generated?
   (b) What correlation can be found between the simulated noise data expressed in EPNL and L_A?
   (c) What are the limitations and restrictions of this correlation?
2. Can a similar relationship be found between the EPLN and SEL metrics?

The search for a relationship between the acoustic metrics is contained in the two main research questions. The first main question is broken down into three sub questions, which act as intermediary steps in answering the main question.
The first sub question will guide the development of the aircraft noise simulation framework. Since aircraft noise touches many disciplines this question is broken down along the four principal disciplines, which are aircraft noise, aero engines, flight trajectories, and aircraft models. Each of these questions touches a discipline in the simulation of aircraft noise and will determine which methods and models will be used.
To answer the second sub question the aircraft noise simulation framework will be used to simulate aircraft flyovers. The simulated noise from these flyovers will then be analysed to determine whether a relationship exists between the EPNL and L_A metrics.
The limitations and bounds of this relationship will be subject of sub question three, as it is important to know the applicability of this relationship for use in future research.
The second main question will investigate the relationship between EPNL and SEL using the methods developed while answering the first main question. A similar breakdown into sub questions could be shown but is not done for the sake of conciseness.

When these research questions are answered it will be possible to give the value of A-weighted decibels for a

certain aircraft during the early conceptual design stages based on the estimated EPNL noise value and certain aircraft parameters. Furthermore the development of the noise prediction framework will grant both the FPP and ANCE departments the capability to include aircraft noise as a discipline into the conceptual design of aircraft. However, let's start with the basics. Therefore, the next chapter will introduce the noise metrics EPNL, L_A, and SEL.

3

Aircraft Noise Metrics

During the development of acoustics and aeroacoustics, researchers have applied numerous methodologies to quantify noise. The dawn of the jet aircraft in the fifties spurred the development of metrics as the contemporary jet engines were much louder than the propeller aircraft at that time. This resulted in the development of acoustic metrics that could capture the human response to aircraft noise [9].

Although there are many different acoustic metrics available, this study will focus on just three of them: L_A, SEL, and EPNL. The first one, L_A, is a weighted acoustic metric based on loudness as perceived by the human ear. The A-weighted sound pressure level falls under the category of community noise metrics. The same can be said of the Sound Exposure Level, SEL, which is a time integrated version of L_A, often denoted by L_{AE}. Both are discussed in Section 3.1. The third one, EPNL, also commonly known as the certification metric is annoyance based and is discussed Section 3.2.

3.1. Community Noise Metrics

For this study two commonly used community noise metrics were analysed. Both L_A and SEL are based on the same weighting method of the SPL level, the difference being that SEL is a time integrated measure of L_A. The weighting and L_A metric are explained in Subsection 3.1.1. The time integration to obtain the SEL metric can be found in Subsection 3.1.2.

3.1.1. A-Weighted SPL or dB(A)

The A-weighted Sound Pressure Level (A-weighted SPL or L_A) is one of the most commonly used metrics in aerospace and environmental sciences. It is often used for the measurement of outdoor environmental noise. Therefore it is often called *"community noise"*. The wide array of applications extends from transportation noise from roads, rail and aircraft to the noise measuring device on the wall of your favourite club.

Its widespread use comes from the fact that the A-weighted SPL is believed to better represent the loudness, as perceived by the human ear, of acoustic phenomena. In fact the human ear perceives signals of high frequency to be louder than signals of lower frequency. This phenomenon can be seen in the equal loudness contours presented in Figure 3.1 where curves of equal phon levels show signals of a specific frequency and SPL level that have the same loudness. For example one can see that a low rumbling signal of 30 Hz and 100 dB will have a phon value of 60 which is equal to a higher signal of 1 kHz at 60 dB.

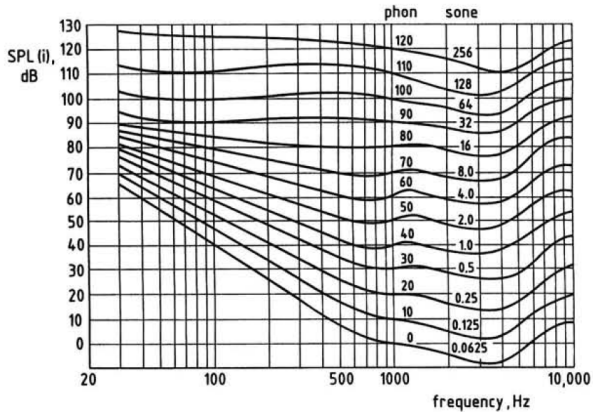

Figure 3.1: Equal loudness contours for pure tones [2]

With this perceived loudness in mind, the A-weighting of the SPL was developed. The 40 phon contour as seen in Figure 3.1 was chosen as reference. At lower frequencies, it can be seen that the SPL level has to be quite high in order for the noise to be perceived to be equally loud as a higher signal. As such, the weighting is higher at lower frequencies, then drops in the range of 200 Hz to 1000 Hz before picking up again at frequencies higher than that. This behaviour can be seen in Figure 3.1. Furthermore this is illustrated by giving the A-weighting for 1/3 octave frequency bands in Table 3.1:

Table 3.1: A-weighting per 1/3 octave band

1/3 octave center frequency [Hz]	A-weighting correction [dB]	1/3 ocatve center frequency [Hz]	A-weighting correction [dB]
50	-30.2	800	-0.8
63	-26.2	1000	0
80	-22.5	1250	0.6
100	-19.1	1600	1
125	-16.1	2000	1.2
160	-13.4	2500	1.3
200	-10.9	3150	1.2
250	-8.6	4000	1
315	-6.6	5000	0.5
400	-4.8	6300	-0.1
500	-3.2	8000	-1.1
600	-1.9	10000	-2.5

The A-weighted sound pressure level is thus a single-event instantaneous metric which is adjusted to the

loudness of certain frequencies as perceived by the human ear. Its computation is quite easy as it only requires the correction of the SPL value with the A-weighting, resulting in this metric being widely used for outdoor noise measurements.

3.1.2. Sound Exposure Level (SEL or L_{AE})

Since the A-weighted decibel is an instantaneous metric, it does not incorporate the effect of signal duration. The Sound Exposure Level (SEL) tries to account for this by integrating the noise impact in dB(A) over time. The result is a time integrated single event metric, where the A-weighted SPL is integrated over the duration for which the noise level is within 10 dB(A) of the maximum dB(A) value. For the integration a normalizing time constant of 1 second, T_1, is used resulting in the definition of SEL according to Equation 3.1:

$$L_{AE} = 10log_{10}\left[\frac{1}{T_1}\int_{t_1}^{t_2} 10^{\frac{L_A(t)}{10}}\,dt\right] \tag{3.1}$$

where, L_{AE} is the SEL value, T_1 the normalizing time constant of 1 second, and t_1 and t_2 specify the time interval in which the time-varying noise impact $L_A(t)$ is within 10 dB(A) of its maximum value. Under this formulation the SEL value expresses a constant sound level which has the same amount of acoustic energy in 1 second as the whole event.

3.2. Certification Noise

The history of certification for aircraft noise started in the fifties in the United States. More precisely in New York, where airline operators wished to introduce the new Boeing 707 at JFK airport (then Idlewild). The increment and difference in noise to contemporary propeller aircraft resulted in public concern. As a consequence, the New York Port Authority and Federal Aviation Administration (FAA) funded research into this topic. This led to the development of aircraft noise certification by using annoyance based metrics and the very first noise abatement procedures [9].

Today the metric used for aircraft noise certification is the Effective Perceived Noise Level (EPNL). This metric uses a lengthy methodology in which it is derived from the Perceived Noise Level metric. This methodology is described in Subsections 3.2.1 to 3.2.3. Subsection 3.2.4 is a summary of the certification procedure under ICAO Annex 16 standards [16].

3.2.1. Perceived Noise Level (PNL)

The PNL metric is similar in nature to the L_A metric seen in Section 3.1 in the sense that it tries to account for the human perception of various tones. In order to do this, psychoacoustic testing was done resulting in the development of so called 'noisiness' scales as seen in Figure 3.2. These scales were given the unit *Noy*, which can be converted into PNdB, the unit of PNL. For a given 1/3 octave spectrum this conversion is done by applying Equations 3.2 and 3.3:

$$N = n_{max} + 0.15\sum_{i=1}^{m}(n_i) - n_{max} \tag{3.2}$$

$$PNL = 40 + \frac{10log_{10}N}{log_{10}2} \tag{3.3}$$

where n_{max} is the spectrum's maximum Noy value, i indicates the i^{th} band of the spectrum, and m is the number of 1/3 octave bands. A further improvement of this metric led to the tone-corrected version PNLT.

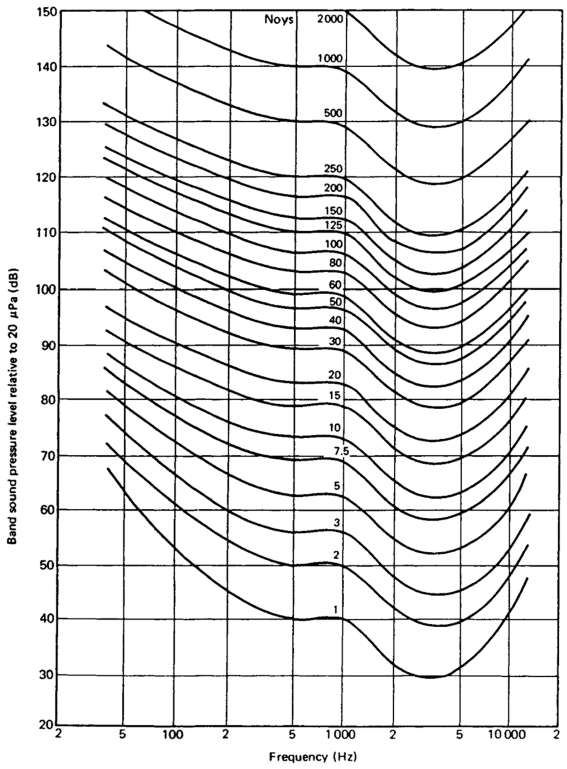

Figure 3.2: Equal noisiness contours [3]

3.2.2. Tone-Corrected Perceived Noise Level (PNLT)

The PNL metric seemed to be quite capable of handling broadband noise. However, tests showed that it did not quite capture the human sensitivity to the presence of discrete tones in the signal. These tones are often perceived to be even more annoying [17]. To take this in account, a tone correction, C, is applied:

$$PNLT = PNL + C \tag{3.4}$$

The value of C depends on both frequency and SPL of the strongest discrete tone in a 1/3 octave band, only considering frequency bands from 80 Hz to 10 kHz. In order to obtain the correction value C, a few steps have to be taken. The first step is calculating the change in SPL, s, of the 1/3 octave bands. This is done starting with the third band (80 Hz) for all 24 bands:

$$s(3) = Novalue \tag{3.5}$$

$$s(i) = SPL(i) - SPL(i-1) \tag{3.6}$$

The second step is comparing this change in SPL to the changes for the previous 1/3 octave bands. If the change is greater than 5 dB it is marked:

$$|\Delta s(i)| = |s(i) - s(i-1)| > 5 \tag{3.7}$$

The marked values of s are then subjected to three tests:

1. If the marked value $s(i)$ is positive and greater than $s(i-1)$, then $SPL(i)$ becomes marked
2. If the marked value $s(i)$ is smaller than or equal to zero, and $s(i-1)$ is positive, then $SPL(i-1)$ is marked
3. If the previous cases do not apply, no value is marked

The fourth step consists of several sub-steps based on the fact whether the SPLs are marked or not. The goal of this step is to find the adjusted sound pressure level, $SPL'(i)$:

1. For all non-marked SPL values, the adjusted sound pressure level equals the original SPL, i.e. $SPL'(i) = SPL(i)$

2. For the marked SPL values the adjusted sound pressure level can be found by:

$$SPL'(i) = \frac{1}{2}[SPL(i-1) + SPL(i+1)] \tag{3.8}$$

3. Note that for marked SPL values, the arithmetic average of the nearby SPLs is taken. This is not possible for the sound pressure level of the 24^{th} 1/3 octave band. When the SPL of this band is marked, the adjusted SPL is calculated as follows:

$$SPL'(24) = SPL(23) + s(23) \tag{3.9}$$

After obtaining the adjusted sound pressure levels, the fifth step makes use of them by calculating the adjusted change values, s'. Note that an s' value has been included for a (non-existing) 2^{nd} band:

$$s'(3) = s'(4) \tag{3.10}$$

$$s'(i) = SPL'(i) - SPL'(i-1) \tag{3.11}$$

$$s'(25) = SPL'(24) \tag{3.12}$$

The sixth step is the calculation of an arithmetic average for three adjacent adjusted change values for the bands $i = 3$ to $i = 23$:

$$\bar{s}(i) = \frac{1}{3}[s'(i) + s'(i+1) + s'(i+2)] \tag{3.13}$$

The seventh step sees another recalculation of the 1/3 octave SPL values for bands $i = 3$ to $i = 24$. These values are the background SPL values:

$$SPL''(3) = SPL(3) \tag{3.14}$$

$$SPL''(i) = SPL''(i-1) + \bar{s}(i-1) \tag{3.15}$$

The eight step consists of calculating the so-called protrusion levels, i.e. the differences $F(i)$ between the original SPL values and the background values:

$$F(i) = SPL(i) - SPL''(i) \tag{3.16}$$

These values are used to determine the correction factor C by using Table 3.2. Note that only difference values, $F(i)$, greater than 1.5 dB are considered to be relevant, all others are ignored. The ninth and final step is the application of Equation 3.4.

Table 3.2: PNLT tone correction factors, C

Frequency, f [Hz]	Level difference, F [dB]	Tone correction, C [dB]
$50 \leq f \leq 500$	$1.5 \leq F < 3$	$F/3$-0.5
	$3 \leq F < 20$	$F/6$
	$20 \leq F$	3.333
$50 \leq f \leq 500$	$1.5 \leq F < 3$	$2F/3$-1
	$3 \leq F < 20$	$F/3$
	$20 \leq F$	6.667
$50 \leq f \leq 500$	$1.5 \leq F < 3$	$F/3$-0.5
	$3 \leq F < 20$	$F/6$
	$20 \leq F$	3.333

3.2.3. Effective Perceived Noise Level (EPNL)

The final step in the derivation of EPNL is taking into account the effect of duration. The reasoning is that the longer people are exposed to noise close to the PNLT maximum the more they will be annoyed. To take this into account a time integration is performed in which values up to 10 dB below the maximum peak are considered, as seen in Figure 3.3. The result is a single event metric which can be obtained using the following equation:

$$EPNL = PNLT_{max} + D \tag{3.17}$$

$$D = 10log_{10}[\sum_{k=0}^{2d} 10^{PNLT(k)/10}] - PNLT_{max} - 13 \tag{3.18}$$

where $PNLT_{max}$ is the maximum peak value of PNLT and D is the duration correction which corresponds to the time interval d in which all values are within a range of 10 PNTdB of $PNLT_{max}$. The index for each time step is k, with each time interval being 0.5 seconds wide (for certification purposes). Normalization for the 10 second interval yields the value 13 (i.e. $10log_{10}(0.5/10)$).

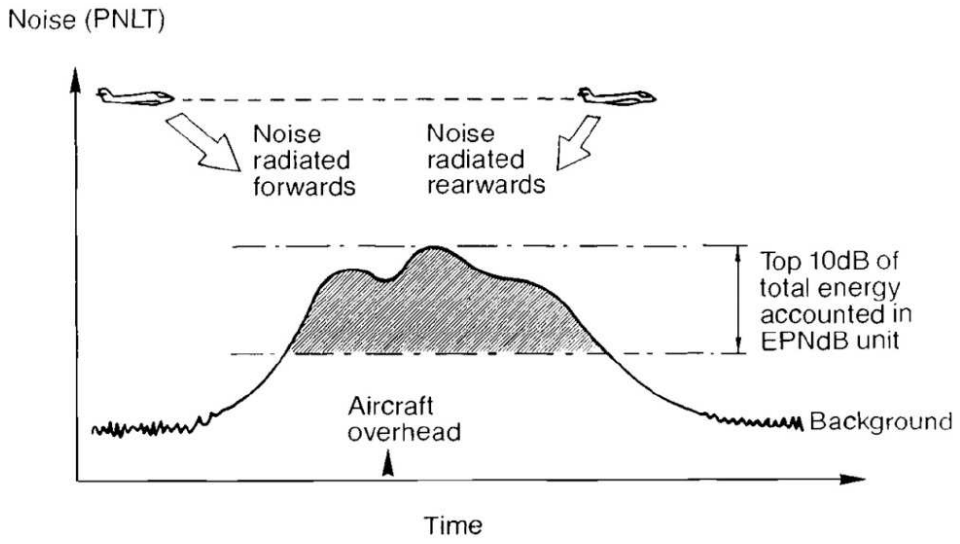

Figure 3.3: Duration correction interval [3]

3.2.4. ICAO Noise Certification

Certification for aircraft noise is done using the procedure stipulated in ICAO Annex 16 [16] (also for FAA and EASA certification). This procedure uses the EPNL metric and measures the emitted aircraft noise during departure and approach stages of flight. This is done using measurements on three microphone locations as seen in Figure 3.4 and explained below:

- **Flyover:** this point is positioned directly under the take-off flight path at 6.5 km from the brake release point
- **Sideline:** this point corresponds to the location which experiences the highest noise measured at a lateral distance of 450 meters from the runway axis
- **Approach:** This point is located directly under the approach flight path at 2 km from the runway threshold

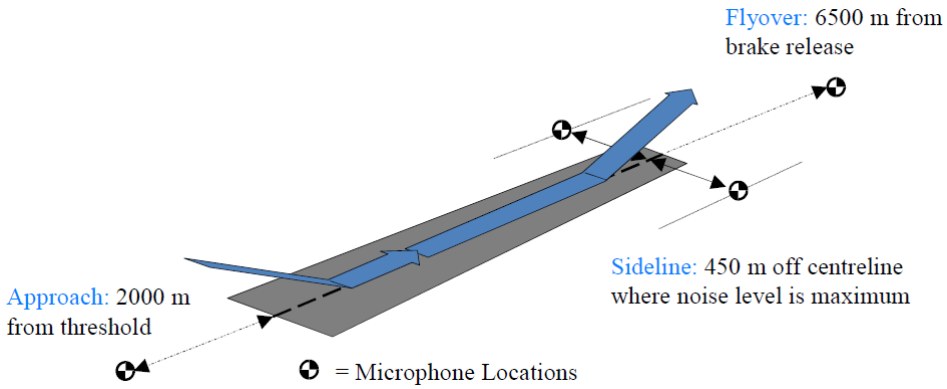

Figure 3.4: ICAO noise certification points [4]

The certification noise level of the aircraft is then the sum of the measured EPNL level at the three locations:

$$EPNL_{certif} = EPNL_{TKO} + EPNL_{LAT} + EPNL_{APP} \tag{3.19}$$

where the subscripts TKO, LAT, APP stand for take-off (flyover), lateral (sideline), and approach, respectively. The aircraft is said to be in compliance with noise certification if this summation is lower than a given limit. These limits are stated in the chapters of annex 16. With the current applied limit being that of chapter 4 (to be replaced by chapter 14 for aircraft designs which will be type certificated in 2017). The limits for each microphone location according to chapter 3 are given by Equations 3.20 to 3.22. Also note the dependency on Maximum Take-Off Weight (MTOW). The cumulative limit for various chapters is given in Figure 3.5. Note that the limit of chapter 4 is that of chapter 3 minus 10 EPNdB, cumulative. The local limits remain equal to those of chapter 3.

$$EPNL_{TKO} = \begin{cases} 89 & for MTOW \leq 48.1 \cdot 10^3 kg \\ 69.65 + 13.29 \cdot log_{10} MTOW & for 48.1 \leq MTOW \leq 385 \cdot 10^3 kg \\ 106 & for MTOW \geq 385 \cdot 10^3 kg \end{cases} \tag{3.20}$$

$$EPNL_{LAT} = \begin{cases} 94 & for MTOW \leq 35 \cdot 10^3 kg \\ 80.87 + 8.51 \cdot log_{10} MTOW & for 35 \leq MTOW \leq 400 \cdot 10^3 kg \\ 103 & for MTOW \geq 400 \cdot 10^3 kg \end{cases} \tag{3.21}$$

$$EPNL_{APP} = \begin{cases} 98 & for MTOW \leq 35 \cdot 10^3 kg \\ 86.03 + 7.75 \cdot log_{10} MTOW & for 35 \leq MTOW \leq 280 \cdot 10^3 kg \\ 105 & for MTOW \geq 280 \cdot 10^3 kg \end{cases} \tag{3.22}$$

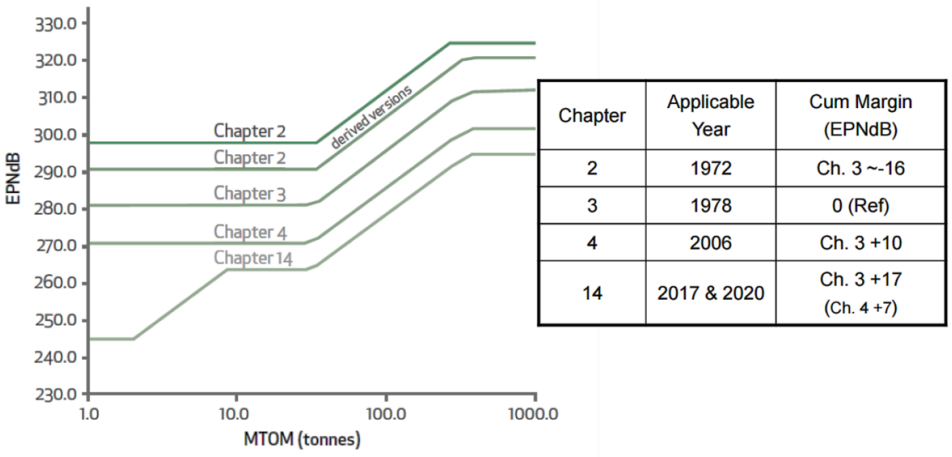

Chapter	Applicable Year	Cum Margin (EPNdB)
2	1972	Ch. 3 ~-16
3	1978	0 (Ref)
4	2006	Ch. 3 +10
14	2017 & 2020	Ch. 3 +17 (Ch. 4 +7)

Figure 3.5: ICAO noise certification cumulative limits [5]

4

Aircraft Noise

Aircraft noise is a complex subject combining many different aspects of acoustics. This is largely due to the many different noise sources on an aircraft. From the tonal whine of the fan to the loud broadband rumbling of the jet, each emitted noise has it's own creation mechanism and influencing parameters. This chapter provides an answer to the questions "What is aircraft noise?" and "How can you model aircraft noise?". The answer to these question is given in steps. The first step is identifying the major noise components of the aircraft, which is done in Section 4.1. This section also introduces the noise simulation program INSTANT, which is used during this thesis. However the noise heard close to an aircraft does not sound similar to that of an aircraft which is far away. As the noise travels from aircraft to observer it will experience a range of absorption and attenuation effects. These effects are described in Section 4.2. All inputs for INSTANT are summarised in Section 4.3.

4.1. Aircraft Noise Sources

Taking a look at the aircraft as a whole, two major categories of noise can be identified, namely *airframe noise* and *engine noise*. This is illustrated by Figure 4.1, where each noise component is identified. On the airframe side you will find that most sources are aerodynamic surfaces such as the slats, flaps, wing and stabilizer. An exception to this is the noise emitted by the deployed landing gear. Note that the noise emitted by antennas and cavities are are considered to be minor sources of airframe noise, hence they are not included in this figure. The engine is responsible for a wide scale of noises from different components. The most prominent being the fan and jet, other key contributors are the low pressure (LP) compressor, the combustor, and the LP turbine.

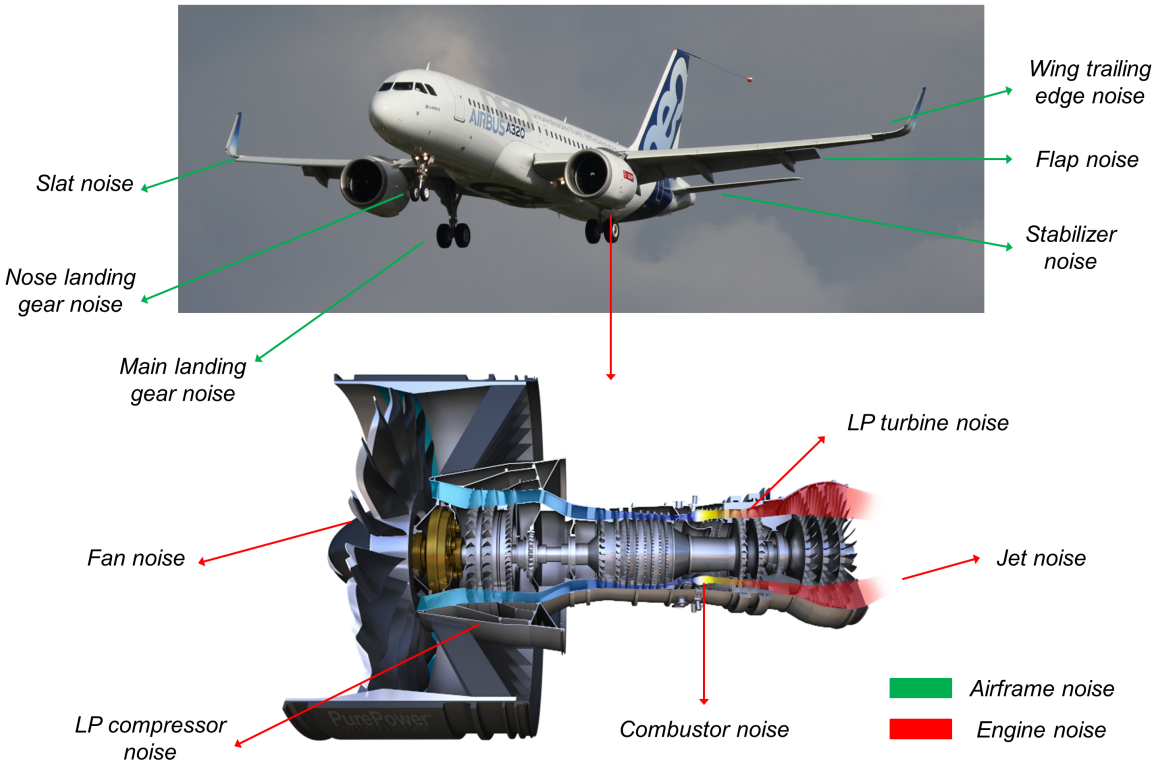

Figure 4.1: Breakdown of the aircraft into noise generating components in INSTANT[1]

The share between airframe noise and engine noise is dependent on the stage of flight (i.e. thrust setting). During take-off, when the thrust setting is high, the engine noise will be dominant with both fan and jet being its main contributors. Contrary to take-off the engine is in a low (near idle) thrust setting during approach. As a result the airframe noise is equivalent to the engine noise. This is mainly due to a large reduction in jet noise at near idle thrust settings. Both the take-off and approach stages are illustrated in Figure 4.2. Note that, due to ongoing research in the field of aircraft noise, this figure is likely to be somewhat outdated. As most research was focussed on the reduction of jet and fan noise, it is likely that other components such as the turbine are becoming more prominent.

[1] Aircraft photograph by author, engine diagram from reference [18]

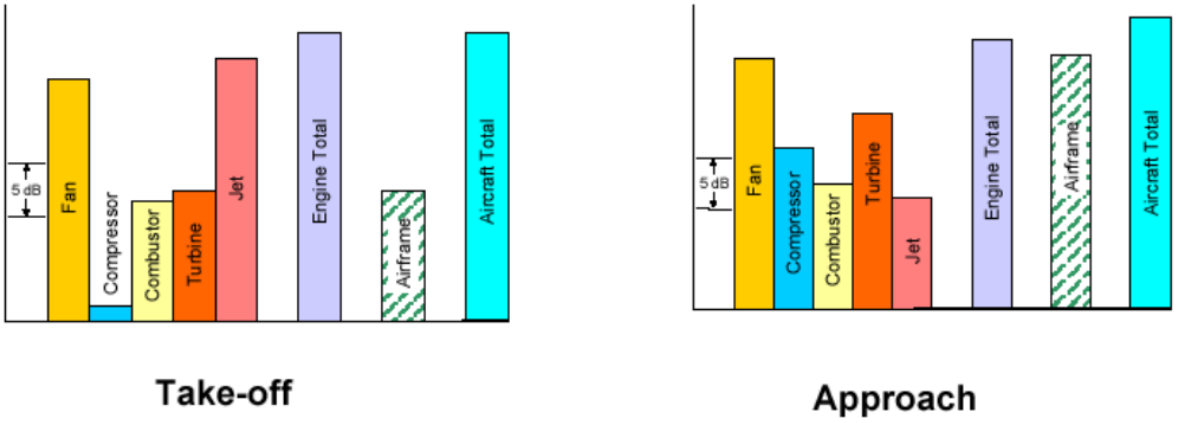

Figure 4.2: The share of airframe and engine noise during take-off and approach [6]

With the sources identified, it is time to take a look at the mechanisms responsible for the emitted noise and how they can be modelled. This is done in the following subsections where INSTANT is introduced and each noise source, corresponding mechanisms and models are discussed.

4.1.1. INSTANT

The simulation of aircraft noise is the core task in this project. For this task the noise simulation program INSTANT was selected, which is a noise simulation and assessment module developed at ILR Aachen by A. Sahai [4]. The key principle of the tool is that it bundles several parametric aircraft component noise models into a single source model for the entire aircraft, allowing fast computation and prediction. It therefore reflects the methodology used in the well known Aircraft Noise Prediction Program (ANOPP) [19], which was developed by NASA.

INSTANT provides an aircraft noise prediction and assessment environment with several interesting features and capabilities. Developed to assist in multidisciplinary aircraft design, INSTANT provides the option of both assessing the noise impact on certification level as well as by calculation of noise contours. The following metrics can be used during these noise simulations:

- A-Weighted decibels (dB(A))
- C-Weighted decibels (dB(C))
- Sound Exposure Level (SEL)
- Perceived Noise Level (PNL)
- Tone corrected Perceived Noise Level (PNLT)
- Effective Perceived Noise Level (EPNL)

Furthermore the noise prediction environment is also able to provide an assessment of the sound quality metrics:

- Loudness
- Sharpness
- Tonality

To achieve these noise predicions, the aircraft is modelled as a single source model of which the noise emission is a summation of the contribution of several noise components. The airframe noise is modelled using the method of Fink [20], which accounts for the wing slat noise, wing trailing edge noise, wing flap noise, stabilizer noise, nose landing gear noise, and main landing gear noise. For the engine noise, the fan and LP compressor contribution are given by the method of Heidmann [21], the combustor noise by the method of Emmerling [22], the LP turbine contribution is accounted for by the method of Matta [23], and finally the jet noise is covered by the method of Stone [24].

While these parametric models have the advantage of being fast, they come with some disadvantages. The main disadvantage can be found in their applicability. The engine models are limited to standard turbofan engines, but even within this category limitations can be found. For example, the Heidmann's fan noise model cannot be used for engines with three spools, nor for the calculation of fan noise in geared turbofan engines. It was also seen that this model heavily overestimates the fan noise for very big bypass ratio engines such as the GE90. Further limitations derive from the number of models available. An example of this is the lack of a model to account for engine shielding, and models for future aircraft concepts such as counter rotating open rotors (CRORs). However, since INSTANT is relatively flexible, these models can be added in the near future.

4.1.2. General Model Form

The individual noise component models and sources are described in the following Subsections. All these models have been adapted to a general form by Zorumski for use in ANOPP [19], on which INSTANT is based. In this form the mean-square acoustic pressure $< p^2 >$ is described by Equation 4.1:

$$< p_{i,j}^2 >= \frac{\Pi_i}{4\pi r^2} \frac{S(\eta)_i D(\theta,\psi)_i}{(1 - M_\infty cos\theta)^4} \rho_\infty c_\infty \tag{4.1}$$

where i indicates the i^{th} noise source of component j and ∞ indicates freestream conditions. Π_i is the acoustic power function of the source i, $S(\eta)$ is the spectral weighting function either dependent on frequency parameter η for most engine components or Strouhal number S for the airframe components, and $D(\theta,\psi)$ is the directivity function. These three functions are specific to each model and their noise sources and can be found in [4], [20], [21], [22], [23], and [24]. The effect of forward flight is accounted for by the factor $(1 - M_\infty cos\theta)^4$. When the aircraft is in motion this factor increases the magnitude of the acoustic pressure. When the mean-square acoustic pressure is known for all sources of a component, it can linearly be added and converted to SPL using Equation 4.2, where the reference pressure p_{ref} has a value of $2 \cdot 10^{-5}$ Pascal:

$$SPL_j = 10 log_{10} \frac{< p_j^2 >}{p_{ref}^2} \tag{4.2}$$

Note that in these models all broadband noise components are seen as 1/3 octave band data, the tonal components however are computed at their exact discrete frequencies. Therefore the frequencies of the tonal components are rounded to the nearest 1/3 octave band frequency since all ANOPP and INSTANT models use the 1/3 spectral band format.

4.1.3. Airframe Noise

Fink's airframe noise model [20] is used to predict the broadband noise and aerodynamic noise created by the airframe. The model consists of a combination of empirical and analytic functions. The measurements for the empiric functions were gathered during several aircraft flyovers with the engines set to idle. The following noise components are accounted for and will be explained: nose and main landing gear noise, slat noise, flap noise, clean wing trailing edge noise, and stabilizer noise. The latter one is taken into account using an adapted form of the functions used for the clean wing trailing edge noise.

The general form of the mean-square pressure equation for airframe components is given by Equation 4.3:

$$< p_{i,airframe}^2 >= \frac{\Pi_i}{4\pi r^2} \frac{F(S)_i D(\theta,\psi)_i}{(1 - M_\infty cos\theta)^4} \rho_\infty c_\infty \tag{4.3}$$

The formula above is nearly identical to the form given in Equation 4.1. The difference can be found in the term $F(S)_i$, which is the spectral weighting function specific to each airframe component and is dependent on the Strouhal number given by Equation 4.4:

$$S = (1 - M_\infty cos\theta)\frac{fL}{M_\infty c_\infty} \tag{4.4}$$

where f is the frequency and L is the characteristic dimension of the airframe noise source. The general form of the acoustic power equation for the airframe noise components is given by:

$$\Pi_i = K_i (M_\infty)^{a_i} G_i \rho_\infty c_\infty^3 b_w^2 \tag{4.5}$$

where K_i is an empirical constant, a_i is a power coefficient, which relates the acoustic power to the free stream flow Mach number. This power coefficient is equal to 5 for bodies which are assumed to be a flat plate or non-compact bodies, such as the clean trailing-edge, and 6 for compact bodies such as a flap. G_i accounts for the effect of the geometry of the airframe component, and b_w corresponds to the aircraft's wingspan.

Landing Gear Noise

Landing gear noise is mostly broadband noise caused by the interaction of the landing gear with the surrounding airflow. It is a complex phenomenon which is highly dependent on the size and configuration of the gear (e.g. strut length, number of wheels, ...). Furthermore, additional noise is created by the interaction of the landing gear and wing and even due to interactions between the wheels themselves. Apart from the broadband noise, a (smaller) tonal component exists, which is caused by flow interaction with objects such as cavities, actuator, and landing gear bay doors.

Clean Wing Trailing Edge Noise

The clean wing trailing edge noise is broadband noise caused by the turbulent boundary layer convection in the wing wake. This process is shown in Figure 4.3. Clean wing trailing edge noise originates from the aircraft's wing and both the horizontal and vertical stabilizers.

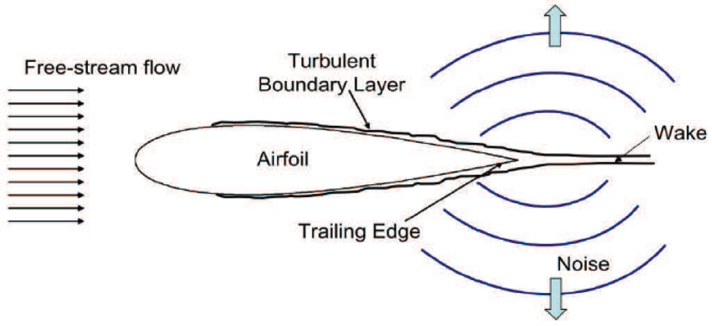

Figure 4.3: Noise mechanism at the trailing edge of an airfoil [7]

Leading Edge Slat Noise

The broadband noise produced by the slats, when deployed, has two main mechanisms: the first one being the trailing edge noise produced by the slat itself, and the second one being an increase in wing trailing edge noise due to the flow over the slat impinging on the wing's boundary layer making it more turbulent.

Flap Trailing Edge Noise

The last airframe noise component is the flap trailing edge noise, which is caused by the turbulent flow of the wing interacting with the flap similar to the flow over the slat interacting with the wing. The intensity and directivity of this noise are highly dependent on the flap configuration and deployment angle.

4.1.4. Engine Noise

Fan Noise

The noise originating from the fan and LP compressor is predicted using the method of Heidmann [21]. This method uses a semi-empirical approach to the complex aeroacoustic phenomena taking place in this engine stage. The following components are accounted for by this method, both radiated in forward and aft direction:

- **Inlet broadband noise:**
  Unsteady or turbulent flow in and around the fan and initial stages results in the aeroacoustic phenomenon known as inlet broadband noise, which is broadband. The sources of these disturbances in the flow can be: inlet flow distortion (IFD) or unsteady flow in the inlet, turbulent boundary layers, blade wakes, and vortices.

- **Discrete tones from inlet:**
  Lift fluctuations on the rotor or stator blades generate discrete tones in the inlet. The source of these disturbances is the blades passing through the wakes originating from the inlet guide vanes or by the wakes from the blades impinging on the stator vanes. These disturbances are periodic as they occur with each fan blade passage, therefore their fundamental frequency is the Blade Passage Frequency (BPF). Higher harmonics persist at integer multiples of the BPF.

- **Combination tones from inlet (or 'buzz-saw' tones):**
  Another component of fan and LP compressor noise is the so called 'buzz-saw noise' or more eloquently put, the combination tones. This noise derives its name from the similarity to the noise generated by a sawmill or 'buzz-saw'. These tones are formed when the rotor blades have such rotational velocity that the relative tip Mach number becomes supersonic. When this is the case, shock waves will be formed at the leading edge of the blades, which will propagate in the forward direction as Mach waves. These waves will coalesce in the inlet duct resulting in cyclic pressure disturbance. This disturbance occurs with each full rotation of the fan rather than each blade passage. As such, the formed combination tones are formed at each multiple of the shaft rotational speed.

- **Exhaust broadband noise:**
  The noise mechanisms responsible for the exhaust broadband noise are the same as those for the inlet broadband noise, apart from the fact that the presence of inlet guide vanes (IGVs) increases the acoustic power of the emitted broadband noise.

- **Discrete tones from exhaust:**
  Discrete tones propagate in aft direction from the engine bypass exhaust. These tones are caused by the same mechanisms as for the discrete inlet tones.

The mean-square acoustic pressure for Heidmann's fan noise model is given by Equation 4.6:

$$< p_{i,fan}^2 >= \frac{\Pi_i}{4\pi r^2} \frac{S(\eta)_i D(\theta)_i}{(1 - M_\infty cos\theta)^4} \rho_\infty c_\infty \tag{4.6}$$

where Π_i is once more the acoustic power of the noise source, $S(\eta)$ is the noise component's specific spectral weighting function, with η as frequency parameter, given by Equation 4.7, $D(\theta)$ is the directivity function, and the term $(1 - M_\infty cos\theta)^4$ is the forward flight effect.

$$\eta = (1 - M_\infty cos\theta) \frac{f}{BPF} \tag{4.7}$$

$$BPF = N \cdot B \tag{4.8}$$

where BPF, the Blade Passage Frequency is the product of the LP spool rotation speed N and the number of fan rotor blades B. The term $(1 - M_\infty cos\theta)$ accounts for the Doppler effect, which is a consequence of the forward flight of the aircraft.

The directivity for fan noise does not vary with azimuth angle ϕ, contrary to the airframe noise. This holds for all engine components as they only vary with polar angle θ and are therefore radially symmetric. Both the spectral and directivity functions derive from observations and measurements carried out by NASA for various fans. Heidmann's original model was found to over-predict the intensity of fan tones. Therefore the method was updated twice by Kontos [25] [26], with the second update accounting for the effect of acoustic liners used in most modern high bypass ratio engines. Both updates are applied in INSTANT.

Information on all relevant functions, parameters and corresponding values can be found in references [4], [19], and [21].

Combustor Noise

Research into combustor noise is still relatively new as it only recently emerged to the foreground due to the reduction of other noise components [27]. The noise produced by the combustion chamber is caused by the fuel heating process and is entirely broadband due to the very turbulent nature of this process. A direct transfer of noise occurs due to gas expanding in the chamber. This gas interacts with the local flow, producing sound waves. Indirect noise is caused by the convection of entropy fluctuations from the combustion chamber to the turbine stages.

Turbine Noise

Due to the geometrical similarities between the compressor and turbine, the noise mechanisms are similar; cyclic pressure disturbances or lift disturbances are caused due to the blade wake interacting with stator vanes which is the source of discrete tones, where as unsteady flow around the rotor and stator is the root cause of broadband noise emitted from the turbine. In most cases, only noise emitted by the low pressure turbine is relevant as noise emitted by the high pressure (HP) turbine does not radiate effectively out of the turbine.

Jet Noise

The final aircraft noise component included in INSTANT is the jet noise. This source is one of the more dominant ones onboard and is particularly present on take-off and other high thrust settings. In the early days of jet aviation this noise source was the most dominant and investigations into this noise by Lighthill led to development of modern aeroacoustics [28]. For the implementation of jet noise into INSTANT the model of Stone was selected, which is used in ANOPP as well [24] [19]. The advantage of this semi-empirical model is that its roots are close enough to the physics of the jet noise problem to give sufficiently accurate predictions, while still allowing for parametric input variation to analyse many different engine configurations [4]. Furthermore does the model of Stone allow for predictions of the jet mixing noise as well as shock induced noise of both turbojet and turbofan engines, although only aircraft with turbofan engines will be considered for this thesis. The model also provides a distinction between engines with a single stream and engines with a coaxial nozzle. More information can be found in references [4], [19], and [24].

As briefly mentioned before there are two jet noise mechanisms: the jet mixing noise and shock induced noise. The latter is not present in the modern jet engines under consideration thus it will not be discussed. The jet mixing noise however is present and originates from the high-velocity jets from the core (primary) and bypass (secondary) mixing with each other as well as with the ambient air. The resulting turbulence causes a broadband rumbling noise in the low frequency range, generally 100-200 Hz for modern turbofan engines [4]. This mixing process is illustrated in Figure 4.4:

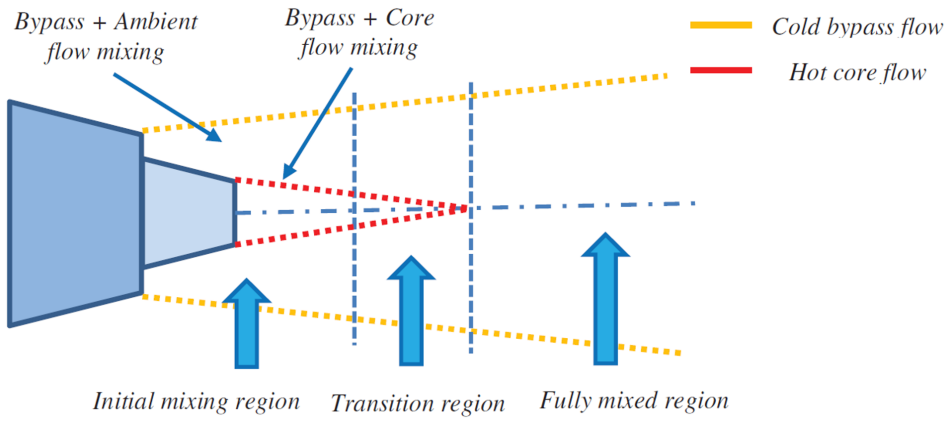

Figure 4.4: The various jets emerging from the engine and their mixing regions [4]

The mean-square pressure of jet noise model takes a different form than the other noise components and is shown in Equation 4.9. The equation for the primary jet and the equation for the secondary jet are the same (apart from the subscript 1 and 2):

$$< p_{jet}^2 >= \frac{< p^2(l_{ref}, 90°) >}{4\pi r^2} \left[\frac{1 + \left(\frac{0.124 v_{j,1}}{c_\infty}\right)^2}{\left(1 + \frac{0.6 \cdot v_{j,1} cos\theta}{c_\infty}\right)^2 + \left(\frac{0.124 v_{j,1}}{c_\infty}\right)^2} \right]^{\frac{3}{2}} D_m F_m H_m G_c G_p \tag{4.9}$$

where $< p^2(l_{ref}, 90°) >$ is the mean-square pressure at a reference length l_{ref} from the nozzle exit for $\theta = 90°$, $v_{j,1}$ is the primary jet velocity, D_m is the directivity function, F_m is the power function for spectral weighting, and H_m is a correction for the forward flight effects. Correction for the far-field pressure disturbance of a coaxial nozzle is done by the factor G_c with the factor G_p correcting for a plug nozzle. More information can be found in references [4], [19], and [24].

4.2. Aircraft Noise Propagation and Attenuation

. With all noise mechanisms known, it is now clear how aircraft noise is formed at the source. However, before the sound waves reach the observer, they still need to cross a reasonable distance through the atmosphere. While doing this these waves are subject to various effects such as geometric spreading, atmospheric absorption, and ground reflection.

Geometric Spreading

Let's assume that the aircraft is a point source. As a result, sound waves will propagate in a uniform fashion in all directions, i.e. spherical spreading. Since the acoustic power radiated from the source remains constant, the sound pressure level will reduce when travelling further away from the source. This is proportionate to the factor $1/r^2$ where r is the distance between the source and the observer. This occurrence is called the inverse-square law and as a consequence a doubling in observer distance will lead to a reduction of 6.02 dB in SPL.

This would be the case in ideal free field conditions. Unfortunately in the real world nothing is ideal. As the distances between aircraft and observer are in general large, the atmosphere in between cannot be considered as being uniform. In general there are many wind and temperature gradients between the aircraft and observer which can curve the sound path. This might lead to the formation of so called 'shadow zones', i.e. regions where the sound waves do not travel [29].

Atmospheric Absorption

Apart from geometric spreading, sound waves are further attenuated by atmospheric absorption. This phenomenon has two main causes: absorption due to viscous effects and the absorption attributed to the molecular composition of the atmosphere. The latter is due to the energy exchange between nitrogen and oxygen molecules in air from their translational, rotational, and vibrational modes as the sound waves pass by [30, 31]. The atmosphere will absorb higher frequencies stronger than lower frequencies. This is illustrated by the fact that you will often hear the low rumbling jet noise over a large distance but not the fan noise.

Ground Reflection and Attenuation

When the sound waves have passed through to atmosphere and reach the observer, they usually reach the ground at nearly the same time. When this happens, they reflect on the ground and a portion will reach the observer, who perceives both the original sound waves and the (slightly delayed) reflected sound waves. The reflected sound waves undergo a change in spectrum and/or attenuation of the original noise. The attenuation depends on the incidence angle of the ground normal axis and the aircraft, and on the surface characteristics (the complex acoustic impedance). INSTANT uses a model based on the Chien-Soroka theory [32] combined with the Delany and Bazley impedance function [33] to estimate the ground reflection and attenuation. The latter provides an estimation of the impedance based on the incident sound's frequency and the effective flow resistivity of the ground. In this case the ground is modelled as a uniform plane and the source is a point source. The resulting geometry is shown Figure 4.5, where θ is the angle of incidence. It is clear that the sound radiated by the source can follow two possible paths to the observer: the direct path r_1 and the indirect path by reflection r_2.

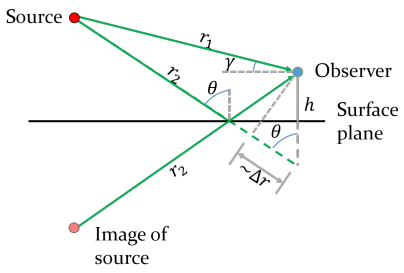

Figure 4.5: Representation of ground reflection and attenuation

Combined Effects

The combined effects of geometrical spreading, atmospheric absorption and ground reflection can be seen in Figure 4.6, which shows the noise spectra for the take-off of a short-range aircraft measured at a distance of 453.2 m. Due to the geometrical spreading over this distance, the signal experiences a uniform reduction of 53.1 dB as can be seen by comparing Figure 4.6 a and b. The effect of atmospheric absorption in Figure 4.6 c is less obvious, because for frequencies below 2000 Hz it only yields minor SPL reductions. Frequencies higher than 2000 Hz however are drastically dampened, with frequencies over 5000 Hz being reduced to values below 50 dB while being originally around 125 dB. Finally the characteristic 'spikes' and 'dips' resulting from ground reflection are added in Figure 4.6 d.

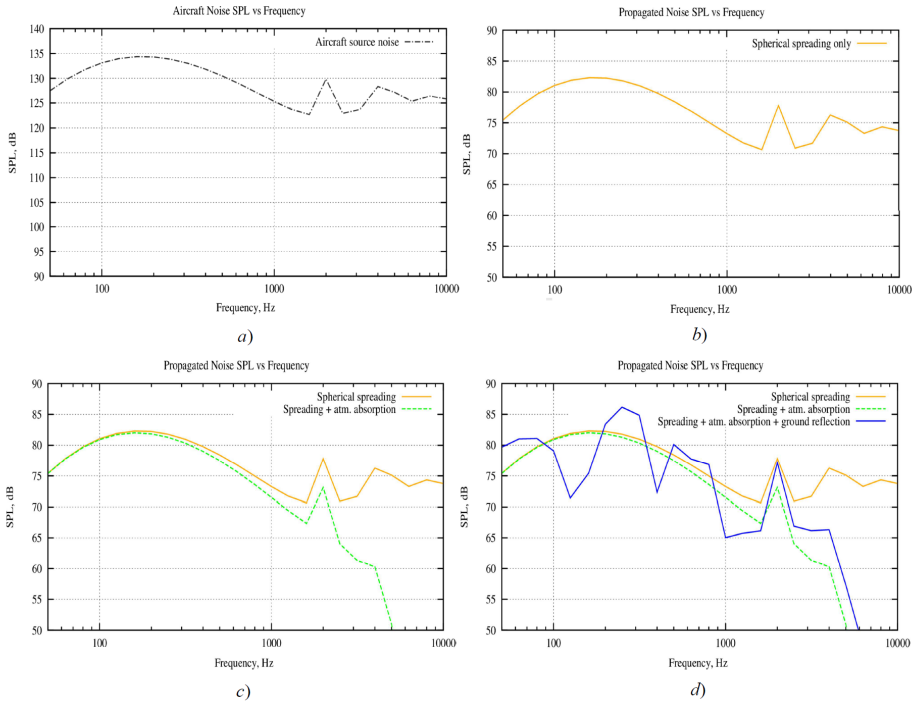

Figure 4.6: The effects of spreading, atmospheric absorption and ground reflection on the noise spectra [4]

This chapter gave insight to the acoustic phenomena at play in aircraft noise. However aircraft noise is defined by many contributing factors ranging from the size of your aircraft to the engines and to the flown trajectory. In order to simulate aircraft noise, these factors require simulation as well. The following chapter explains the methodology used in achieving a noise simulation framework.

4.3. Summary of INSTANT Inputs

INSTANT requires two types of inputs: geometric and operational. Geometric inputs are fixed during the flight such as the wingspan, whereas the operational inputs, such as turbine inlet temperature (TIT), will vary. An overview of the inputs can be found in Table 4.1:

Table 4.1: Summary of the inputs required for INSTANT

Geometry Inputs		**Operational Inputs**	
Parameter	*Symbol*	*Parameter*	*Symbol*
Main gear wheel diameter	d_{MG}	Landing gear setting	-
Nose gear wheel diameter	d_{NG}	Slat setting	-
Main gear strut length	l_{MG}	Flap setting	-
Nose gear strut length	l_{NG}	Flap deflection angle	δ_f
Wing span	b_w	Fan mass flow rate	$\dot{m}$
Wing area	A_w	Fan (LP) rotational speed	$N1$
Horizontal tail span	b_h	Total temperature rise across fan	ΔT
Horizontal tail area	A_h	Combustor entrance mass flow rate	$\dot{m}_{comb.}$
Vertical tail span	b_v	Combustor entrance total temperature	$T_{t,i}$
Vertical tail area	A_v	Combustor exit total temperature	$T_{t,j}$
Flap span	b_f	Combustor entrance total pressure	$p_{t,i}$
Flap area	A_f	Combustor exit total pressure	$p_{t,j}$
Fan inlet area	A_{fan}	Turbine (LP) rotational speed	N
Number of rotor blades	B	Turbine entrance total temperature	$T_{t,i}$
Number of stator vanes	V	Turbine exit static temperature	T_j
Fan rotor diameter	d	Primary jet Mach number	$M_{j,1}$
Fan rotor tip Mach number at design point	$M_{t,d}$	Secondary jet Mach number	$M_{j,2}$
Rotor-stator spacing	s/C	Primary jet temperature	$T_{j,1}$
Inlet Guide Vane index	IGV	Secondary jet temperature	$T_{j,2}$
Combustor entrance area	$A_{comb.}$	Primary jet velocity	$v_{j,1}$
Turbine rotor diameter	$d_{turb.}$	Secondary jet velocity	$v_{j,2}$
Turbine inlet area	$A_{turb.}$	Primary jet density	$\rho_{j,1}$
Turbine blade number	$B_{turb.}$	Secondary jet density	$\rho_{j,2}$
Primary jet area	$A_{j,1}$	Aircraft altitude	h_a
Secondary jet area	$A_{j,2}$	Observer altitude	h_o
Plug diameter	d_p	Distance	r
Engine inlet axis angle	δ	Airspeed	V

A large part of these inputs are engine geometry variables such as the fan inlet area and the number of rotor blades. These parameters are estimated by INSTANT using empirical relations based on sea-level-static thrust [4]. Other parameters provided by INSTANT are the landing gear, flap, and slat settings. These are currently scheduled in INSTANT's code. The remaining parameters have to be provided to INSTANT by the remaining simulation programs. The aircraft geometry is provided by Initiator, the engine parameters by GSP, and the aircraft altitude and airspeed by the trajectory program. These inputs are provided to INSTANT in xml format. The implementation of these programs in the aircraft noise simulation framework is discussed in the following Chapter.

5

Aircraft Noise Simulation and Analysis

The previous chapters introduced the key concepts of aircraft noise and how it is modelled using INSTANT. This chapter will build on that by providing insight in the methodology followed during this thesis project. This methodology can be divided into three parts:

- The simulation programs and simulation framework
- The simulation methodology
- The analysis methodology

The first part will discuss the programs selected for the simulation of aircraft noise. This simulation requires the cooperation of four disciplines. Therefore a framework was put together incorporating an aircraft design program, an engine simulation program, a flight trajectory simulation, and finally the noise simulation program. All these programs where readily available within the ANCE and FPP departments of the Faculty of Aerospace Engineering. These tools and the noise simulation framework are explained in Section 5.1. The second part of this chapter details the chosen methodology for noise simulation. It will explain the reasoning behind the selection of aircraft, engines, and flight profiles. This information can be found in Section 5.2. The verification of the results for the aircraft design, engine, and trajectory programs is shown as well. The third and final part of the methodology corresponds to the analysis of the noise simulations. This analysis investigates the relationships between the EPNL, L_A, and SEL metrics and can be found in Section 5.3.

5.1. Noise Simulation Framework

The simulation of aircraft noise requires many factors and parameters. Most of these are time-dependent variables, which in turn require simulations themselves. To illustrate this, let us look back at Chapter 4. In this chapter it was shown that there are two major components of aircraft noise: engine and airframe noise. The engine noise is highly dependent on the internal thermodynamics of the engine which vary continuously during the flight. This is in contrast to the airframe noise, which is mainly dependent on the constant geometry of the aircraft. Exceptions to this are the deployment of landing gear, flaps, and slats. It can be seen that, in order to properly simulate aircraft noise, these variables need to be known at each point during the flight. In addition to an aircraft noise simulation program, also an aircraft model, an engine model, and a flight trajectory model are required. These three models are each provided by individual programs.

This section deals with the individual programs required to simulate aircraft noise and how they come together as the aircraft noise simulation framework. For this purpose this section is divided in several subsections. As INSTANT was already discussed in Chapter 4 it wont be detailed here. The aircraft design program, Initiator is shown in Subsection 5.1.1, where its capabilities are discussed alongside the inputs and outputs. The same format is used for the discussion of the engine simulation program, GSP, and the flight trajectory program in Subsections 5.1.2, and 5.1.3, respectively. The entire framework is shown in Subsection 5.1.4.

5.1.1. Initiator

One of the goals of this project is to be able to incorporate aircraft noise analysis in aircraft design. To achieve this an aircraft design tool needs to be incorporated into the aircraft noise simulation framework. Since 2011 the FPP department is working on the aircraft design program Initiator [34][35][8]. Initiator translates a set of Top Level Requirements (TLRs) into a conceptual aircraft design, while offering a wide range of capabilities:

- Conceptual design of conventional and unconventional jet aircraft:
  - Tube-and-wing configurations
  - Three-surface configurations
  - Canard configurations
  - Prandtl configurations
  - Blended wing body configurations
- Weight estimation
- Aerodynamic analysis
- Landing gear sizing
- Performance estimation
- Cost estimation
- Key Performance Indicators (KPI) estimation
- Aircraft geometry output (both 2D and 3D)

The computational workflow of Initiator is given in Figure 5.1. The process starts with the definition of the TLRs: payload weights, field lengths and altitudes, range, cruise speed, etc. Furthermore, certification requirements imposed by CS-25 are also implemented into the preliminary design. The next step would be the Class I weight estimation which is based on Torenbeek's method of "lost range" [36]. In this method the Operational Empty Weight (OEW) is estimated based on payload and range requirements coming from a reference database. This database can contain both existing aircraft and designs generated by the Initiator. When this

is done, the most convenient combination of wing loading and thrust-to-weight ratio is selected. Now that the airplane weight and surface area are known, Raymer's method of volume coefficients [37] is used to determine a crude geometry of the aircraft.

Based on this, a convergence loop for Maximum Take-Off Weight (MTOW) is started. During this convergence process weight is estimated using the Class II methods from Raymer [37] and physics based Class II.V methods for wing and fuselage weight [38–40]. The aerodynamic discipline is analysed using the Athena Vortex Lattice (AVL) tool, which is also used for the aerodynamic loads required for the Class II.V weight estimation. Important for this thesis project is that the engine sizing is done using the method of Tang [41] resulting in the required input for GSP. When the MTOW has converged over the iterations of the design loop, the design will be frozen. The resulting design is also subjected to a cost estimation, which is not of interest to this project and will thus be ignored. The long development of Initiator included the work of many students which lead to the inclusion of at least as many functions. A downside of this is that oversight might have been lost as becomes clear in Section 5.2.

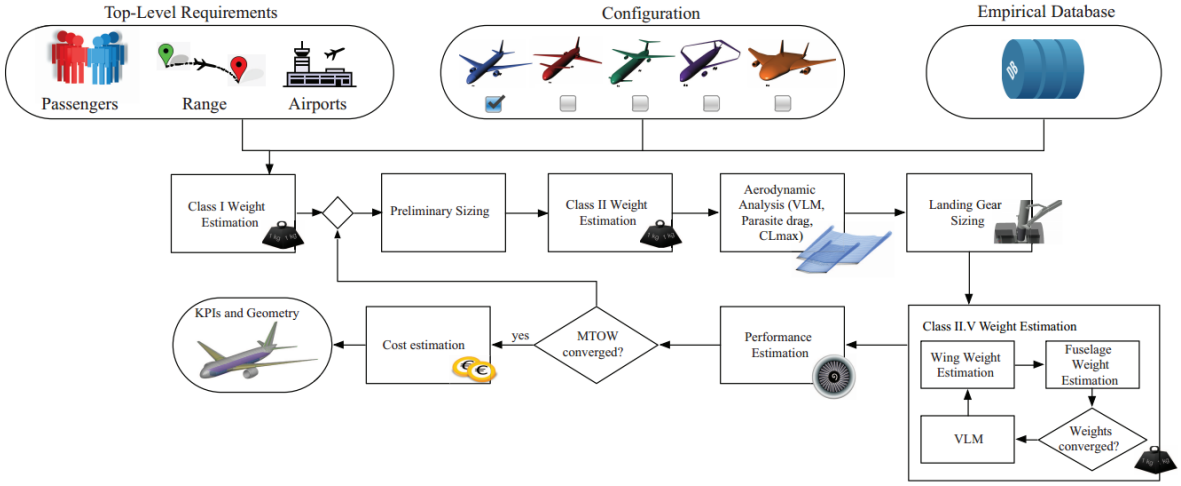

Figure 5.1: Schematic process diagram of the Initiator [8]

As said previously, Initiator generates an aircraft based on a set of given TLRs. This input of TLRs is shown in Table 5.1. The last parameter 'Aircraft configuration' indicates the desired configuration of the aircraft with possibilities ranging from conventional aircraft to prandtl configurations, blended wing bodies, and more.

Table 5.1: The required TLRs input for Initiator

Initiator TLRs input	
Parameter	*Symbol*
Number of passengers	n_{pax}
Passenger class distribution	$n_{classes}$
Payload weight	$W_{payload}$
Cruise Mach number	M_{cr}
Cruise altitude	H_{cr}
Cruise range	R_{cr}
Take-off distance	d_{TKO}
Landing distance	$d_{landing}$
Number of cycles	n_{cycles}
Loiter time	t_{loiter}
Divergence range	R_{div}
Number of engines	$n_{engines}$
Aircraft configuration	–

The design process preformed by Initiator will yield the basic geometry parameters for the aircraft. These parameters are required for Fink's airframe noise model, which is implemented into INSTANT. The aerodynamic and flight performance parameters such as the required thrust, MTOW, lift polars, and others will be fed to the flight trajectory program. However, before the flight trajectory can be discussed, one needs to take a look at the engine simulation software GSP.

5.1.2. GSP

From Chapter 4, it is clear that a large amount of engine variables is required throughout the noise simulation. The majority of these variables are so-called "operational" parameters meaning that they vary during the flight. Therefore a program that is able to model the engine's thermodynamics and simulate these parameters is required. Furthermore this model should assess the fuel consumption of the engine as this is required later on for the flight trajectory calculation. For this purpose the Gas turbine Simulation Program (GSP) was selected.

The Gas turbine Simulation Program is a tool that has been developed gradually at the National Aerospace Laboratory (NLR) and the Delft University of Technology (TUDelft). The development of GSP started around 1986 based on the NASA DYNGEN gas turbine model [42]. Throughout the years, GSP was further developed including the application of object-oriented modelling and the switch from FORTRAN to Delphi's Object Pascal language resulting in the current version, GSP11.

GSP allows for calculation of the gas turbine performance both for a reference design point (DP) as for steady-state off-design (OD) and transient simulations. The simulation is built upon both aero-thermodynamic equations and user specified characteristics for each engine component. The aero-thermodynamic equations are mostly represented by conservation laws and are represented as non-linear differential equations (NDEs).

The main purpose of GSP is to calculate gas turbine performance. The novelty however lies in the object oriented software approach. This object oriented method allows for the creation of generic adaptable models, avoiding models of different engine types from using the same model elements and instead using more accurate custom tailored elements [43]. This custom tailoring of model elements is the Adaptive Modelling (AM) functionality of GSP [44]. This allows for a high degree of flexibility and easy adoption of the code resulting in a relatively easy extension of functionalities. An example of a GSP model is shown in Figure 5.2, which shows an aero engine model composed of several object blocks. Different arrangements of these blocks allow for the analysis of different engine architectures.

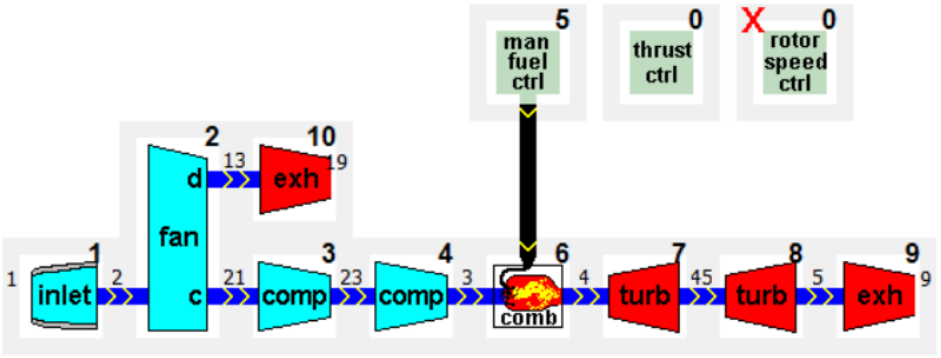

Figure 5.2: GSP model of the CFM56-5B4 engine

The methodology of GSP is based on the well known gas path analysis method [45]. The core mechanism of this method is the analysis of the thermodynamic variables through each engine component (e.g. LP compressor) using aerodynamic and thermodynamic conservation laws. These equations form a system of non-linear differential equations, which is then solved to obtain the engine variables using the Newton-Raphson method. The the conservation laws used in GSP are given below. Some of these conservation laws have time derivatives, which are equal to zero for all steady-state simulations, they are non-zero only for transient sim-

ulations.

The conservation of mass flow through a component is given by:

$$\frac{dM_v}{dt} = W_{in} - W_{out} \tag{5.1}$$

where M_v is the mass in volume V and W is the mass flow with the subscript in and out describing the direction of the mass flow relative to the component. The relations between mass, density, temperature, pressure, and volume V are:

$$M_v = \rho \cdot V_{comp} \tag{5.2}$$

$$\frac{dM_v}{dt} = \left(\frac{1}{RT} \cdot \frac{dp}{dt} - \frac{p}{RT^2} \cdot \frac{dT}{dt}\right) \cdot V_{comp} \tag{5.3}$$

where ρ is the density, V_{comp} the internal volume of the component, R is the specific gas constant, T is the temperature, and p is the pressure. Assuming adiabatic isentropic compression, this relationship becomes:

$$\frac{dM_v}{dt} = \frac{V_{comp}}{\gamma RT} \cdot \frac{dp}{dt} \tag{5.4}$$

where γ is the ratio of specific heats.

The conservation of energy through a component is given by:

$$\frac{dM_v}{dt} \cdot u + M_v \cdot \frac{du}{dt} - Q = w_{in} \cdot h_{in} - w_{out} \cdot h_{out} + PW_{abs} \tag{5.5}$$

where u is the velocity of the mass, Q and PW_{abs} are the heat and power absorbed by the component, h is the specific enthalpy.

The conservation of energy for a drive shaft is given by:

$$I \cdot \frac{d\omega}{dt} \cdot \omega = PW_{abs} + PW_{del} \tag{5.6}$$

where I is the shaft's moment of inertia, ω is the shaft's angular velocity, and PW_{del} is the power delivered by the shaft.

Furthermore, the conservation of momentum for joining flows such as in the combustor (air and fuel) is given by:

$$\sum(w_{in} \cdot c_{in} + A_{in} \cdot p_{s,in}) + F_x = w_{out} \cdot c_{out} + A_{out} \cdot p_{s,out} \tag{5.7}$$

where c is the flow velocity, A is the entrance or exit area of the component (denoted by subscript in or out), p_s is the static pressure at entrance or exit, and F_x is the axial force. An application of this conservation law would be the calculation of the net thrust produced by the core and bypass nozzle. This is illustrated by Equation 5.8:

$$FN = \sum[w_i \cdot (c_{i,8} - c_{00}) + A_{i,8} \cdot (p_{i,8} - p_0)] \tag{5.8}$$

where FN is the net thrust which is the sum of both the thrust generated by the core and bypass, w is the mass flow of the jet, $c_{i,8}$ is the jet velocity, c_{00} is the velocity of the fully expanded exhaust gas, $A_{i,8}$ is the jet area, $p_{i,8}$ is the jet pressure, and $p_{0,0}$ is the pressure of the fully expanded jet.

The conservation laws for all engine components form the system of NDEs that needs to be solved in order to determine the engine performance. The boundary conditions of the problem are derived from the prescribed operating conditions. By default this is done using fuel flow (FF). However in aircraft operations the engine input is often described by a percentage of total thrust. Using total thrust as the input to this problem rather than FF makes this problem implicit as a cycle calculation can return a power setting for a given

FF, but the inverse is not possible. Therefore an extra equation is added to the set of system equations using the FF as extra unknown.

As engine models are quite complex they require a wide range of inputs. This report attempts to give an overview of the most common inputs required by GSP for the simulation of aero engines. Three different types of inputs can be identified: operating envelope inputs, engine component inputs, and control inputs.

This project will require the simulation of engine parameters during take-off and approach, i.e. at varying points in the flight envelope. These points can be defined in the International Standard Atmosphere (ISA) [46] by using two variables: altitude and Mach number. Based on these two variables, GSP is able to derive the other ambient conditions such as air density and static and total air pressure. A third available input is a temperature offset to the reference ISA conditions (by convention 288.15 K at sea level). Furthermore, to simulate the engine parameters over a series of these input variables, a user-defined increment to each variable can be given. The inputs for the operating conditions are given in Table 5.2:

Table 5.2: The operating envelope inputs

Operating envelope inputs	
Parameter	*Symbol*
Altitude	z
Mach number	M_∞
Temperature offset	dT_∞

The second type of inputs are all inputs relating to the individual engine components such as the inlet and compressors. The inputs can be found in Table 5.3. Some components, such as for example the combustor, can either have fuel flow or exit temperature as input (but not both). This is indicated by * for the applicable parameters. Furthermore, one of the assumptions for this project is neglecting the heat sink effect of the engine components. Therefore the associated inputs are excluded from the table.

Table 5.3: The required inputs to define GSP engine components

Component inputs			
Parameter	*Symbol*	*Parameter*	*Symbol*
Inlet inputs		**Combustor inputs**	
Design mass flow	$\dot{m}_{0,des}$	Combustion efficiency	η_{comb}
Inlet pressure ratio	PR_{inlet}	Fuel flow*	$\dot{m}_f$
Inlet area	A_{inlet}	Turbine exit temperature	T_{exit}
Fan inputs		Design point rel. pressure losses	dp_{comb}
Shaft number	$1 or 2$	Duct cross area	A_{comb}
Drive gearbox efficiency	$\eta_{gear_{fan}}$	**Turbine inputs**	
Gear ratio	GR_{fan}	Shaft number	$1 or 2$
Bypass ratio	BPR	Design LP spool speed	$N_{des_{LP}}$
Design rotor speed	$N_{des_{fan}}$	Design HP spool speed	$N_{des_{HP}}$
Core side pressure ratio	$PR_{fan_{core}}$	LP spool mechanical efficiency	$\eta_{mech_{LPturb}}$
Bypass side pressure ratio	$PR_{fan_{bypass}}$	HP spool mechanical efficiency	$\eta_{mech_{HPturb}}$
Core side efficiency	$\eta_{fan_{core}}$	Design efficiency LP	η_{LPturb}
Bypass side efficiency	$\eta_{fan_{core}}$	Design efficiency HP	η_{HPturb}
Compressor inputs		**Exhaust inputs**	
Shaft number	$1 or 2$	Throat area	A_{throat}
Design LP spool speed	$N_{des_{LP}}$		
Design HP spool speed	$N_{des_{HP}}$		
Pressure ratio LP	PR_{LPcomp}		
Pressure ratio HP	PR_{HPcomp}		
Design efficiency LP	η_{LPcomp}		
Design efficiency HP	η_{HPcomp}		

The final category of input are control inputs. These inputs define the operating setting of the engine. In order to achieve consistency in the problem, only one control input can be used at a time. For example, if you set the engine to a certain thrust setting, you cannot alter the fuel flow input as the latter one has become a free variable. The relevant control inputs can be found in Table 5.4:

Table 5.4: The relevant control inputs of GSP

Control inputs	
Parameter	*Symbol*
Fuel flow	FF
Turbine exit temperature	T_{exit}
Fuel to air ratio	FAR
Stator outlet temperature	SOT
Net thrust	FN
Rotor speed	N_1 or N_2

Engine parameters are required at each step in the flight path in order for INSTANT to predict the engine noise as seen in Chapter 4. Since the resolution of the flight trajectory is set at one data point per half second, this can quickly accumulate to a large set of data points. While GSP can simulate the engine performance over a series of inputs, this would be quite computationally expensive. Therefore the approach of creating performance decks seems to be more suitable. Performance decks are data files containing the performance variables of the engine at a range of various operating points. They are created by varying the input variables over a range of possible values. Most often the varied inputs are those defining the operating envelope as seen in Table 5.2 and one of the control inputs given in Table 5.4. The simulation is run for each data point and the results are stored for later use.

It might seem that the creation of the performance deck requires more computational effort than just the simulation of the flight trajectory. This certainly holds true for a single noise prediction. However, if multiple predictions are required with varying flight paths, the approach of performance decks holds the benefit that one deck can be used for multiple trajectories. This way a previously made performance deck can be searched for the engine parameters corresponding to the flight conditions at that point of the simulation, eliminating the need to rerun the engine simulation. Even if the flight conditions do not exactly match those stored in the performance deck, the requested values can still be interpolated from nearby data points.

5.1.3. Trajectory Simulation

With both the aircraft and engine modelled, it is time to bring these two together in the flight trajectory program. The selected tool is the Fokker 100 performance model created by B.J. van Bruchem at the TUDelft in 2015 [47]. Using the Point Mass Model (PMM) approach, this program simulated the entire flight trajectory of a Fokker 100 aircraft in MATLAB. However, for use in this thesis, the program had to be modified to accept the aircraft input from Initiator and the engine input from GSP.

The simulation is based on the use of a point mass model with Newtonian mechanics. The problem can be divided into two separate stages: a ground roll phase and an airborne phase. The ground roll phase is only relevant during take-off and landing, while the aircraft is on the runway. The ground roll phase is only a small segment of the envisioned mission as the ground roll is often in the order of one to three kilometres. It does define the point where the aircraft becomes airborne and thus the shape of the noise contours near the runway. However, as the airborne phase of the flight covers a considerably larger area, its influence on the noise contours is more pronounced. For the use of Newtonian mechanics the following assumptions were made:

- The aircraft is a point mass, thus all forces are assumed to act at the center of gravity of the aircraft and all mass inertia effects are ignored
- The aircraft is assumed to be in trimmed condition
- The line of thrust is assumed to be parallel to the centerline of the fuselage, hence α_T equals α

- Lateral and longitudinal motion are assumed to be decoupled, the validity of this assumption holds for small deviations
- Engine bleed air effects are neglected, hence the performance of the aircraft is somewhat overestimated
- Control lag is neglected, hence all control inputs take place instantaneously
- The atmosphere is considered to be the International Standard Atmosphere [46]

With these assumptions the equations of motion (EOM) can be derived for both phases. Starting with the ground roll phase, the EOM can be derived from Figure 5.3:

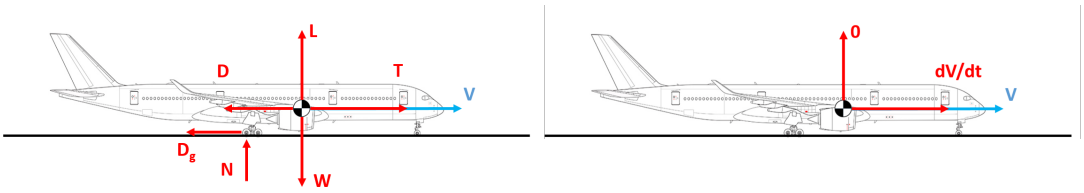

(a) Free body diagram (b) Kinetic diagram

Figure 5.3: Free body and kinetic diagrams of the aircraft during ground roll

Searching force equilibrium parallel to V gives:

$$\sum_{\parallel V} T \cdot cos\alpha_T - D - D_g = m\frac{dV}{dt} \tag{5.9}$$

where T is the aircraft's thrust, D is the drag force caused by the atmosphere, D_g is the drag force from runway friction, L is the lift force, W the aircraft's weight, N the normal force, m is the mass of the aircraft, and V is the aircraft's velocity. The same approach, but now perpendicular to V gives:

$$\sum_{\perp V} L + N + T \cdot sin\alpha_T - W = 0 \tag{5.10}$$

The breakdown of forces and accelerations for the airborne phase is shown in Figure 5.4:

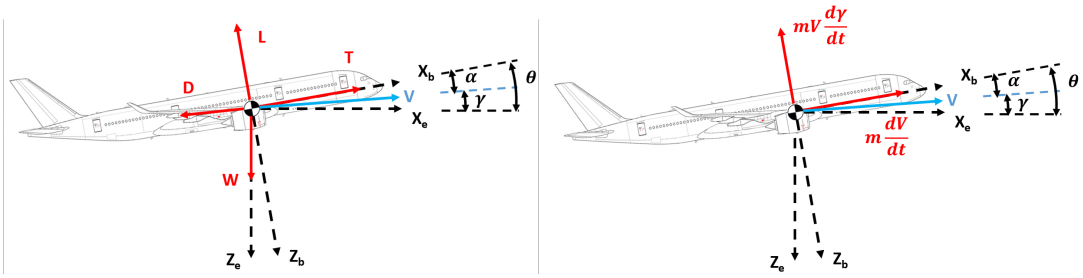

(a) Free body diagram (b) Kinetic diagram

Figure 5.4: Free body and kinetic diagrams of the aircraft during flight

Applying Newton's second law of motion, the sum of forces parallel to the velocity vector gives:

$$\sum_{\parallel V} T \cdot cos\alpha_T - D - W \cdot sin\gamma = m\frac{dV}{dt} \tag{5.11}$$

where γ is the flight path angle which is equal to the pitch angle θ minus the angle of attack α. Summing of forces perpendicular to V yields:

$$\sum_{\perp V} L - W \cdot cos\gamma + T \cdot sin\alpha_T = mV\frac{d\gamma}{dt} \tag{5.12}$$

The flight trajectory program made use of the flight manual of the Fokker 100. Meaning that digitalised plots were used for engine input and aerodynamic input. This also means that currently the program is limited to jet aircraft and does not allow for the use of propeller aircraft. The main revision for this program was implementing the use of the Initiator and GSP output as input for the trajectory program. A downside of using Initiator input is that at the moment Initiator does not have a properly functioning high lift devices module. As a result, the improved trajectory model offers no estimation of the effect of using high lift devices. Another adaptation was that the program made use of the engine pressure ratio (EPR) as control input for thrust and fuel flow. Since INSTANT requires the primary spool speed $N1$ as input, it was decided to adapt the trajectory program to use $N1$ as well. The final adaptation of the program was done with respect to the procedures to be flown during take-off and approach, but these are further discussed in Section 5.2. The overall inputs of the flight trajectory program and where they originate from are given in Table 5.5:

Table 5.5: The main inputs of the trajectory program

Flight Trajectory Input		
Input	*Examples*	*Origin*
Mission	Payload weight, range, ...	Initiator
Aerodynamic	lift and drag polars	Initiator
Aircraft geometry	MTOW, wingspan, ...	Initiator
Engine	Thrust, fuel flow, ...	GSP

As output, this program will deliver the flight trajectory of the aircraft, meaning the x-coordinate (distance) and the z-coordinate (altitude) along with the airspeed of the aircraft. In combination with the output from Initiator and GSP, everything is now available for the noise simulations.

5.1.4. Aircraft Noise Simulation Framework

The previous subsections introduced the programs required for the noise simulations along with their in- and outputs. The theoretical interlinking of this in- and output is shown in Figure 5.5. The aircraft is generated by Initiator based on the top level requirements, after which it is fed to the point mass model. Meanwhile, the aircraft's geometry is passed on to the airframe noise module of INSTANT. In parallel the engine simulation is performed by GSP and the resulting engine deck is transferred to the point mass model. The engine thermodynamics are fed to the engine noise module. The flight trajectory program then computes the trajectory and feeds the relevant information to INSTANT, which calculates the source noise for each mission point based on a resolution of 0.5 seconds. The next step in the process is the propagation of the noise and the application of absorption and attenuation effects. This is done in order to calculate the noise for each observer point. The final step is the assessment of the aircraft noise in which both certification and community noise can be assessed.

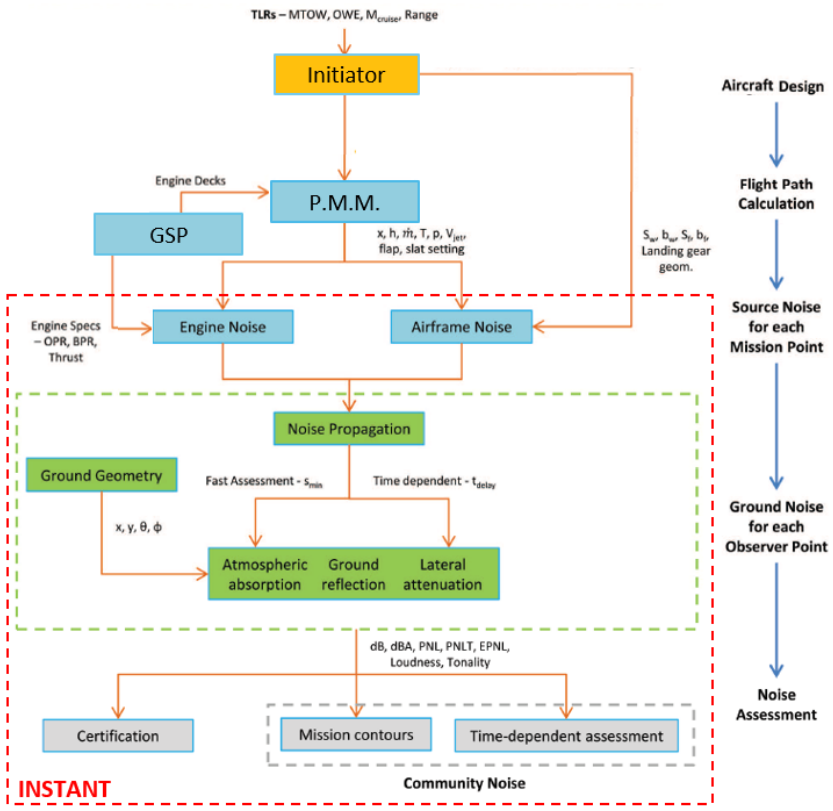

Figure 5.5: The theoretical implementation of the framework

The practical implementation differs slightly from the theoretical implementation as can be seen from the simplified image in Figure 5.6. The aircraft designed by Initiator is stored as a MATLAB data-object which is loaded by the point mass model in MATLAB. The GSP engine decks are exported in text format and converted to CSV format after which they can be imported into the point mass model. This point mass model can be seen as the compiler of all required inputs. After calculating the flight trajectory the point mass model will write the XML flight trajectory files required for INSTANT, which contain: the location of the aircraft, the flight conditions, and engine thermodynamics for each point on the flight trajectory. These XML files are then read by INSTANT, which in itself is a C++ application.

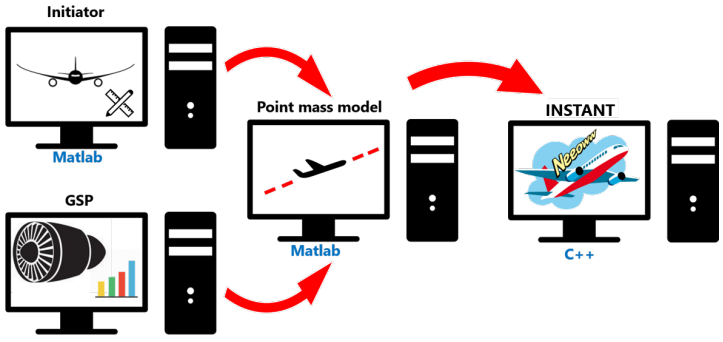

Figure 5.6: The practical implementation of the framework

5.2. Simulation Methodology

A well defined simulation approach is required to obtain proper results. In this case there are three main aspects to the simulation:

- The aircraft selection

- The engine selection

- The definition of the flight trajectory procedures

Aircraft Selection

For the first aspect it was argued that the selected aircraft should range from small to large covering a large area of the currently existing aircraft. In Chapter 4 it was seen that INSTANT is limited to conventional wing-fuselage aircraft with the engines mounted under the wing. This is therefore reflected in the selection. The following aircraft have been selected:

- Fokker 100

- Airbus A320

- Airbus A330-300

- Long range aircraft 1 (LR 1)

- Long range aircraft 2 (LR 2)

These aircraft cover most of the current market and available sizes. Furthermore, the selected engines cover a suitable range of thrust and bypass ratio, ranging from 67.2 kN to 513.9 kN of thrust and a bypass ratio (BPR) of 3 to 7. All of these aircraft have wing mounted engines, except for the Fokker 100 (F100). For the purpose of this project, it is assumed that this aircraft has wing mounted engines instead of fuselage mounted engines. Originally only Initiator designed aircraft were to be used in the simulations. However, the results from Initiator showed that these designs did not always reflect reality, as can be seen in Table 5.6. For small aircraft such as the F100 and A320, the results were quite close. However, Initiator failed to replicate this for the long range aircraft 1 and 2. Due to the complexity of the Initiator it is not quite clear what causes the discrepancy for these two aircraft. Therefore it was chosen to simulate the reference aircraft as well using the aerodynamic results from the Initiator versions. This brings the total amount of simulated aircraft to 10. Furthermore for the A330, long range aircraft 1, and long range aircraft 2 it was seen that Initiator estimated landing gear strut lengths longer than 7 meters, since this was unreasonable they were replaced by the values of the real aircraft.

Table 5.6: Comparison of Initiator results to reality

	Fokker 100			A320		
	Ini.	**Ref.**	**Difference %**	**Ini.**	**Ref.**	**Difference %**
b [m]	29.85	28.08	+6.3	32.45	33.91	-4.3
S [m^2]	105.73	93.50	+13.1	112.14	122.40	-8.4
$l_{fuselage}$ [m]	32.23	32.50	-0.8	35.79	37.57	-4.7
MTOW [t]	44.52	44.50	0.0	71.71	71.50	+0.3
OEW [t]	25.73	24.59	+4.6	38.68	41.31	-6.4
W/S [kg/m^2]	421.06	475.94	-11.5	639.52	584.15	+9.48
T/W [N/kg]	3.02	3.02	0.0	3.05	3.30	-7.6
	A330-300					
	Ini.	**Ref.**	**Difference %**	**Ini.**	**Ref.**	**Difference %**
b [m]	61.80	58.00	+6.6			
S [m^2]	412.40	363.10	+13.6			
$l_{fuselage}$ [m]	64.82	62.47	+3.8			
MTOW [t]	244.91	242.00	+1.2			
OEW [t]	137.17	118.19	+16.1			
W/S [kg/m^2]	593.85	666.48	-10.9			
T/W [N/kg]	2.43	2.46	-1.2			
	LR 1			**LR 2**		
	Ini.	**Ref.**	**Difference %**	**Ini.**	**Ref.**	**Difference %**
b [m]	55.40	47.57	+16.5	73.56	64.80	+13.5
S [m^2]	383.62	283.30	+35.4	623.46	436.8	+42.7
$l_{fuselage}$ [m]	50.42	53.67	-6.1	67.80	73.86	-8.2
MTOW [t]	228.36	186.88	+22.2	426.76	351.54	+21.4
OEW [t]	120.29	86.18	+39.6	217.25	167.83	+29.4
W/S [kg/m^2]	595.27	659.65	-9.8	684.50	804.80	-14.9
T/W [N/kg]	2.34	2.86	-18.2	2.41	2.92	-17.5

Engine Selection

After selecting the aircraft, it was time to pick the right engines. This was done looking at the Ascend fleet database from Flightglobal [48]. For each aircraft type the most common engine was picked. This resulted in the following list for both the actual and Initiator aircraft:

- Fokker 100 powered by Rolls Royce Tay 650-15
- Airbus A320 powered by CFM56-5B4
- Airbus A330-300 powered by CF6-80E1A4
- Long range aircraft 1 powered by CF6-80C2B6F
- Long range aircraft 2 powered by GE90-115B1

These five engines had to modelled in GSP. In order to mimic their performance, they were modelled to reflect the performance recorded in ICAO's emission databank [49], with respect to thrust and fuel flow. During ICAO's tests the engines performance were measured at 4 conditions based on thrust setting: take-off (100 %), climb out (85 %), approach (30 %), and idle (7 %). In GSP the engines where tweaked by changing their design efficiencies and mass flows in order to replicate the thrust and fuel flow recorded in the databank. When possible this was done in a way that the error was less than 10 %. However, more importantly, the primary and secondary jet velocities were kept around 500 m/s and 300 m/s, respectively. This criteria was deemed more important for noise simulation than the 10 % error margin. The results of the modelling can be seen in Table 5.7 and Figure 5.7. All engines meet the error criterion for thrust. For fuel flow, it can be seen that all engines meet the criterion at take-off and climb out, which is reasonable since they have been modelled for these conditions using . As a result the models are slightly less suitable for approach and idle conditions resulting in a slightly larger error, especially for the smaller engines. This behaviour is as expected since the engine was modelled using maps, which are specifically for the take-off and climb-out conditions. Using these standard maps it is not possible to accurately predict the engine's performance at extreme off-design conditions such as idle. The inaccuracies at idle setting are not of importance since this condition is ground idle with 7% N1, while flight idle often occurs around 30% N1. Therefore ground idle will never be occurred during the flight and is a non-issue for the prediction of aircraft noise.

Table 5.7: Engine modelling results

Engine	**Thrust [kN]**	**BPR**	$V_{j,p}$ **[m/s]**	$V_{j,s}$ **[m/s]**
RR Tay 650-15	67.20	3.0	510	303
CFM56-5B4	117.90	5.9	534	301
CF6-80E1A4	297.44	5.1	543	300
CF6-80C2B6F	267.03	5.1	541	300
GE90-115B1	514.17	7.1	549	300

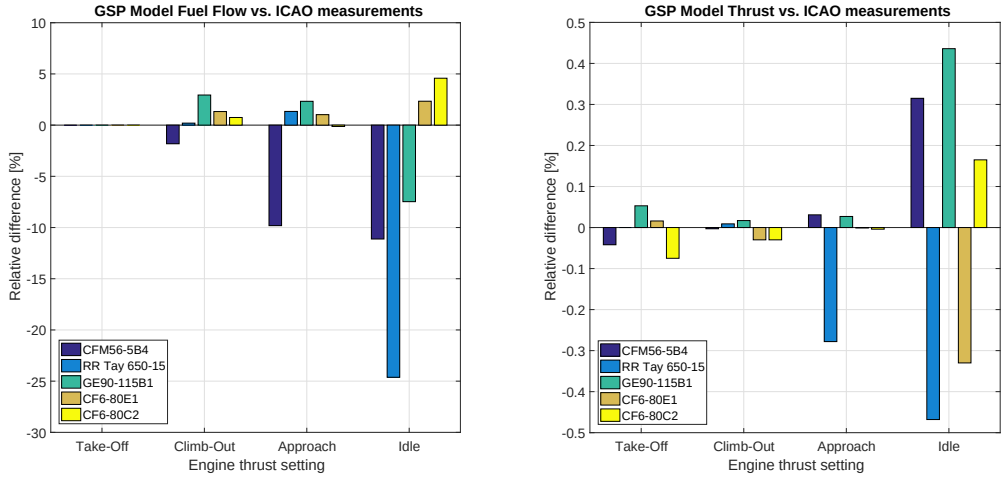

Figure 5.7: The error margin of the GSP models

It was also decided to created two engine decks per engine, one low resolution deck and one high resolution deck. The high resolution deck would be used for the part of the flight under 3000 m, with an altitude step size of 50 m. For altitude higher than 3000 m, the low resolution deck was used with a step size of 500 m. The reasoning behind the use of two decks is that the parts of the flight most relevant to noise are at a low altitude. For the other parts of the flight there is less need for accuracy with respect to noise. Having two resolutions thus decreased the number of data points which were simulated by GSP. During simulations a downside was found to GSP. In some cases, when GSP finished simulations of near idle spool speeds and commenced simulations of full throttle spool speeds the difference in spool speeds, would be so big that the calculations would not converge. This is due to GSP starting convergence either at the design point or the previous off design condition.

Flight Procedures

The final selection required, for defining the simulation methodology was the selection of flight procedures. Since the noise impact of your aircraft is greatly influenced by the way you take off and land, this selection was quite vital to the project. The flight procedures can be split in two categories: departure procedures and approach procedures. Before these procedures could be implemented, the trajectory model had to be adapted so that it could use the GSP and Initiator outputs as input. This was done in two steps. The first step was the implementation of the GSP engine decks as input for all engine related calculations in the trajectory model. The results of the implementation can be seen in Figure 5.8, where the original model is compared to the improved model with GSP input for the Fokker 100:

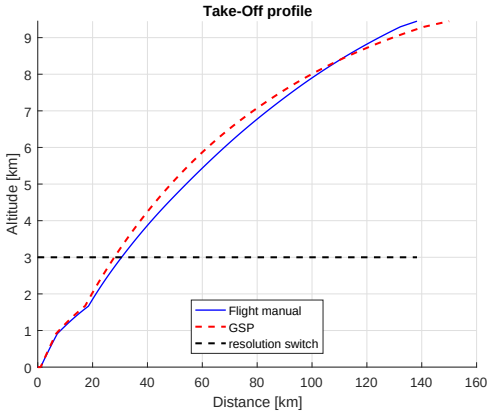

(a) Take-off & climb trajectory

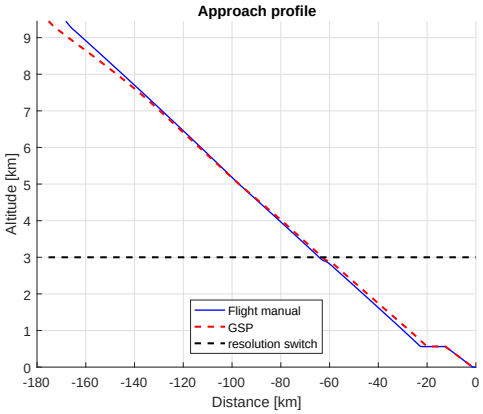

(b) Descent & approach trajectory

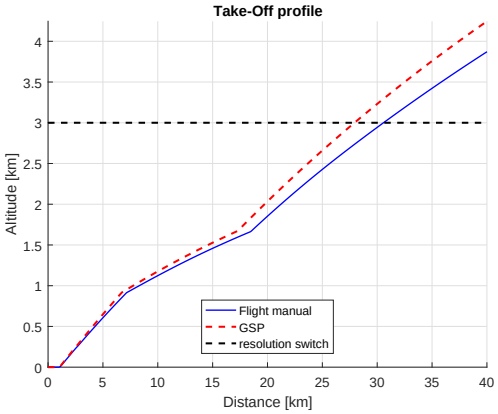

(c) Take-off trajectory

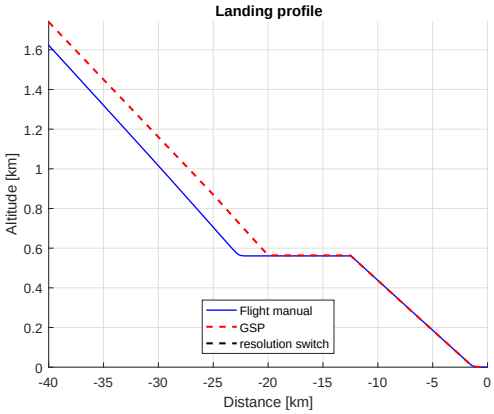

(d) Approach trajectory

Figure 5.8: Comparisson of the trajectory model with GSP and flight manual input

From Figure 5.8 it can be seen that there are two effects at play. Focussing on Figures 5.8a and 5.8c, it is clear that initially the GSP aircraft has a bit more thrust resulting in a faster climb rate. However, as the GSP aircraft nears cruise altitude, its rate of climb decreases and becomes less than the original aircraft. This is most likely due to thrust reduction with altitude which is either overestimated by the GSP model or underestimated by the flight manual. On the approach side, it can be seen in Figures 5.8b and 5.8d that the glide slope for the GSP during descent is more gentle than the flight manual aircraft. During the project it was found that this is due to a programming error in the original flight trajectory model. During descent, when the engine is at near idle conditions, a zero or even negative thrust value was seen in the original model. In reality, the engine still has some thrust during idle in the order of a couple of kilo newtons. The result is that it takes longer for the GSP aircraft to decelerate and descend.

The second step in upgrading would be the replacement of the flight manual input by the Initiator geometry and aerodynamics input to the flight trajectory model. The effects of this replacement is shown in Figure 5.9, where the aircraft based on GSP and Initiator input is compared to the flight manual aircraft:

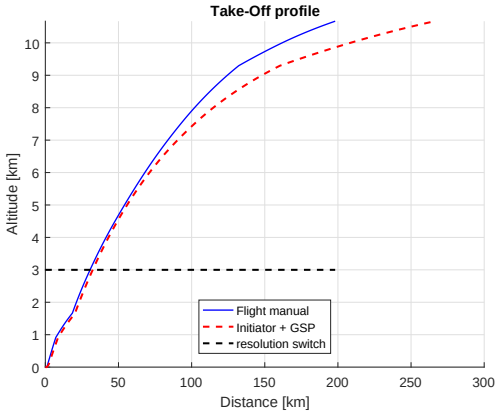

(a) Take-off & climb trajectory

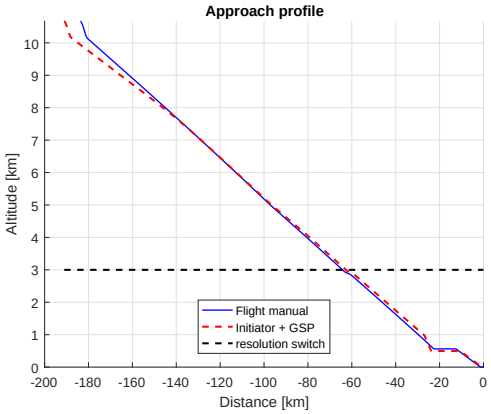

(b) Descent & approach trajectory

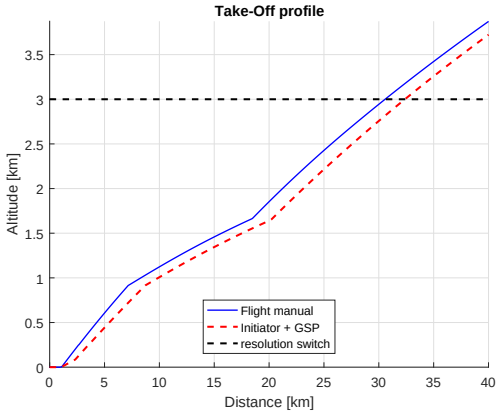

(c) Take-off trajectory

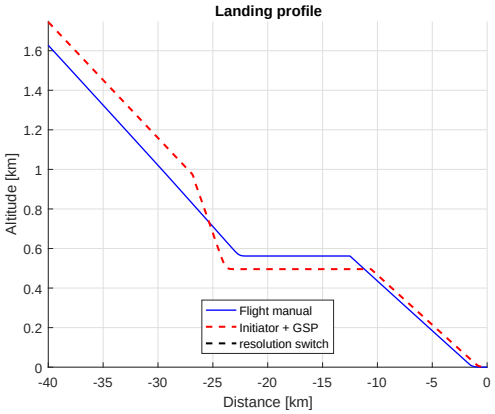

(d) Approach trajectory

Figure 5.9: Comparisson of the trajectory model with GSP and Initiator input versus the flight manual input

When observing Figures 5.9a and 5.9c, it can be seen that the flight manual aircraft climbs faster for the entire duration of the take-off and climb, in contrast to Figure 5.8. This is a consequence of the lower wing loading of the Initiator aircraft as seen in Table 5.6. The same conclusion can be made for Figures 5.9b and 5.8d, where the flight manual aircraft descends faster. Note that in Figure 5.8d, the Initiator aircraft rapidly descends around 25 km from the runway. This was due to a programming mistake which has since been patched, however due to the continuous evolution of the code, this image could not be updated.

The reason for not being able to update Figure 5.8d is the addition of flight procedures to the trajectory model. As mentioned before, flight procedures were added during take-off and landing. Take-off saw the implementation of ICAO's Noise Abatement Departure Procedure 1 (NADP 1) [6], shown in Figure 5.10. This procedure intends to reduce the noise impact close to the runway and is often flown during normal day to day operations. When the aircraft is beneath 800 ft, the engine is at maximum thrust setting. After crossing 800 ft, the thrust setting is reduced to climb setting. The aircraft is in take-off configuration until 3000 ft after which it will change to the clean configuration. Below 3000 ft, a speed limit applies where the aircraft has to stay above V2+10kts and below V2+20kt.

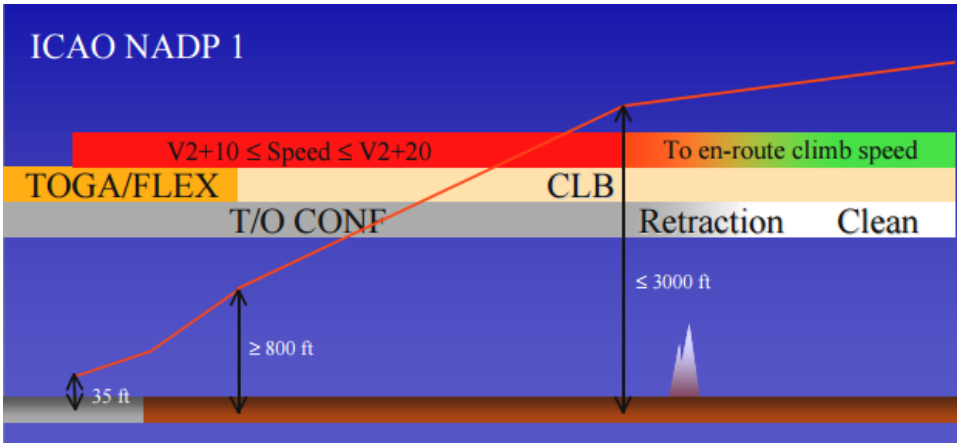

Figure 5.10: ICAO Noise Abatement Departure Procedure 1 [6]

The proposed standard procedure for the approach is shown in Figure 5.11. The first descent of the procedure is done at idle thrust and at the maximum allowed speed for a flightpath angle as steep as possible. The aircraft levels out at 3,000 ft for the level phase of the approach. During this phase the aircraft decelerates to the minimum velocity until the glideslope is intercepted. The final phase is the runway approach in which the aircraft follows the 3° glideslope until touching down on the runway. This procedure was mostly implemented in the trajectory tool but required some upgrading. The results of the implementation of both take-off and approach procedures can be seen in Figure 5.12:

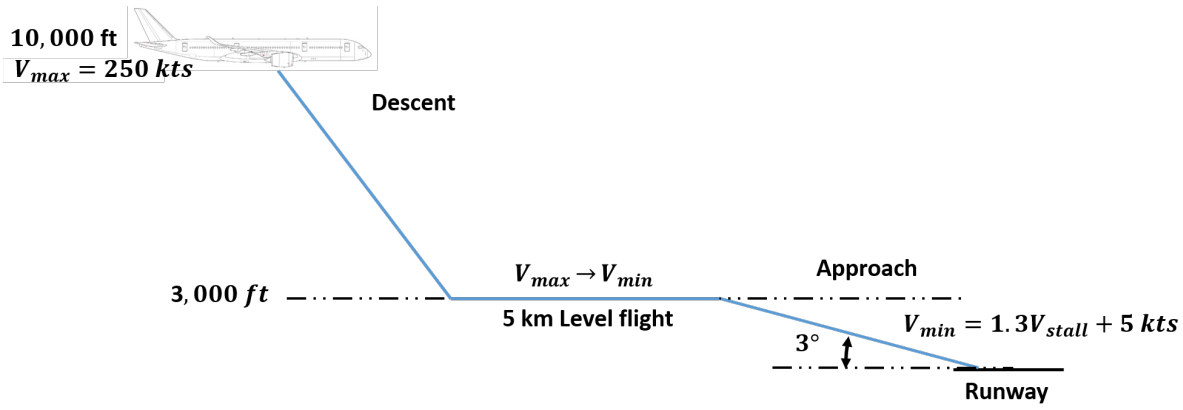

Figure 5.11: The implemented approach procedure

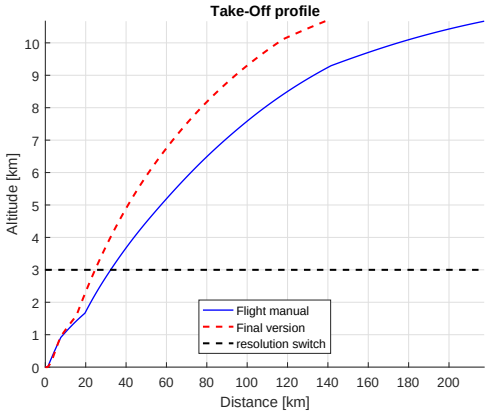

(a) Take-off & climb trajectory

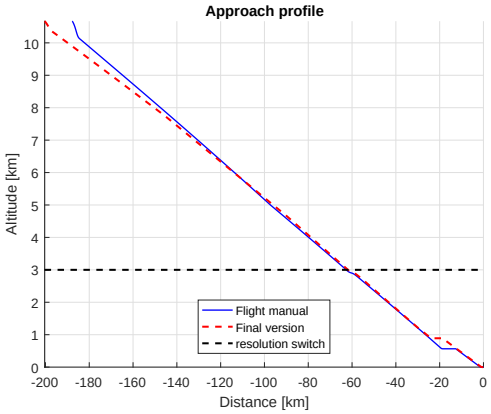

(b) Descent & approach trajectory

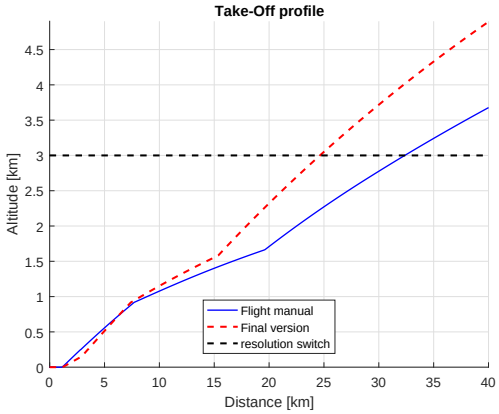

(c) Take-off trajectory

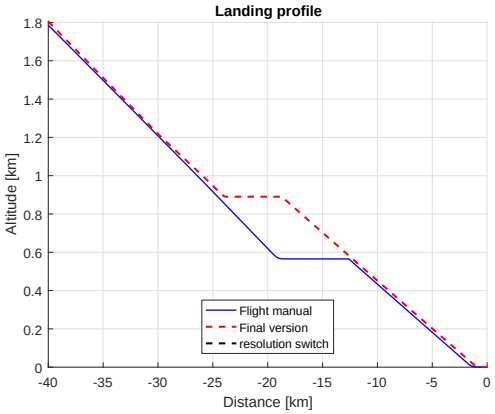

(d) Approach trajectory

Figure 5.12: Comparisson of the trajectory model with GSP and Initiator input versus the flight manual input

In Figures 5.12a and 5.12c the departure trajectory can be seen. The roles of both aircraft have changed and now it is the Initiator version which climbs faster. The main reason for this is an improvement of the GSP model compared to the one used for Figures 5.8 and 5.9. The main improvement of the model is a better interpolation of the engine decks resulting in higher thrust at higher altitudes. The difference in descend slope can still be seen in Figure 5.12b. The change of the horizontal approach from 2000 ft to 3000 ft is also quite clear from Figure 5.12d.

Noise Simulation

With the definition of the aircraft, engines, and flight procedures everything is ready for the noise simulations. To achieve this, the aircraft were created using the Initiator and engine decks where made in GSP. These aircraft and engines were then run through the trajectory model, which compiled all required inputs for the noise simulation in INSTANT. The noise simulation was performed for two outputs:

- The noise certification results
- The EPNL, L_A, and SEL contours

The noise certification process of aircraft was explained in Chapter 3. INSTANT would return the maximum EPNL values at the three certification points. Additionally, INSTANT would calculate the maximum EPNL, L_A, and SEL on a grid of ground point near the runway. Using this data the noise contours could be formed such as the one shown in Figure 5.13.

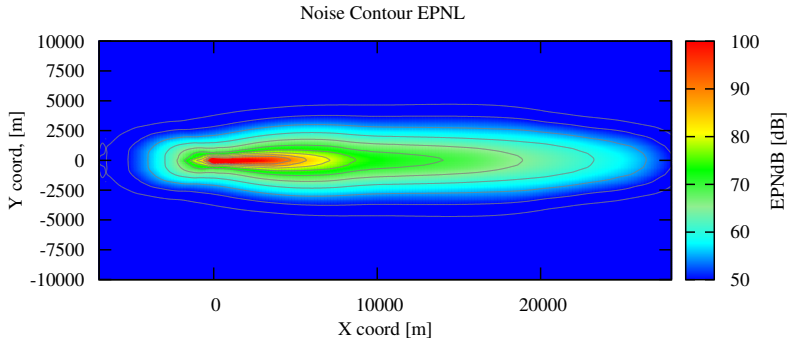

Figure 5.13: The departure EPNL contour for a short range aircraft

5.3. Analysis Methodology

After simulating the aircraft noise, the results have to be analysed. Considering the objective of this project, two aspects can be seen to this analysis. The first is the comparison of the certification values of the simulated aircraft to their real life examples. The second aspect is finding a relationship between the three noise metrics: EPNL, L_A, and SEL.

Certification Noise Analysis

For the analysis of certification noise, the simulation results will be compared to the values recorded in EASA's noise type certificate database [50]. For this purpose the simulated reference aircraft will be compared to their real life counterparts. The Initiator versions of the aircraft are not used in this validation since they do not have a real life counterpart. During the analysis possible differences in flight trajectory and procedures have to be taken into account since aircraft manufacturers often use heavily noise optimised procedures for certification, which are not found in day to day operations. The results of this analysis can be found in Chapter 6.

Metric Relationship

For the assessment of the relationship between the three metrics, all ten aircraft can be used. This can be done because the noise simulations produced by Instant hold true regardless of the existence of the aircraft in real life. Furthermore even if the simulations of INSTANT would be incorrect they can still be used for this analysis as the calculation of the metrics, as shown in Chapter 3 still holds.

The analysis of the relationships can be broken down into three steps:

1. The first step is checking if there is an actual relationship between the EPNL levels of an aircraft at the certification points with the community noise metrics. This can be done by comparing the EPNL levels to the areas contained within the contours. This is done for the 65, 70, 75, 80, and 85 dB(A) or EPNdB contours.

2. The second step investigates the relationship between the contours themselves. This is done by comparing the areas within the contours expressed in EPNL, L_A, or SEL to the areas contained within the contour expressed by one of the remaining two metrics.

3. The third step is to properly define and quantify the relationship, such that it can be used in the prediction and estimation of aircraft noise.

The first step is required to determine the baseline of the acoustic relationships. This step will show whether there is a relationship to be found at all. The second step builds upon this by taking the comparison to contour level. If both of these steps show a correlation between the three metrics it can be said that there is in fact a relationship. Ideally, this relationship would be in the form of Equation 5.13:

$$L_{A_{x,y}} = f(EPNL_{A/C}, MTOW, b, S, l_{fuselage}, T, BPR, x, y) \tag{5.13}$$

where $L_{A_{x,y}}$ is the L_A level at location (x, y), $EPNL_{A/C}$ are the certification levels of the aircraft, $MTOW$ is the maximum take-off weight, b is the wing span, S is the wing area, $l_{fuselage}$ is the fuselage length, T is the maximum thrust of the engine, BPR is the bypass ratio, x is the longitudinal distance from the runway, and y is the lateral distance. Note that this relationship relies on the certification noise level of the aircraft, parameters indicating the size of the aircraft, and parameters defining the engine of the aircraft. The same approach can be used to find a relationship between EPNL and SEL. To summarize, the steps required in finding the relationship are:

1. Correlate the EPNL certification values of an aircraft to the areas within the noise contours
2. Correlate the areas within the noise contours of the EPNL metric to the areas within the contours of the two other metrics
3. Determine if this relationship can be refined to the form given by Equation 5.13

6

Results and Discussion

The previous chapter explained the methodology applied to simulate aircraft noise. This chapter will show you the results of these simulations and provide an answer to the following two questions: "Can the aircraft noise simulation framework be used for noise estimation during conceptual design?" and "Can a relationship be found between the metrics?". The first question will be answered by comparing simulated results to reality, where possible, and checking the reasonableness of the results. This is done in Section 6.1. Answering the second question was the main goal of this thesis and is done in Section 6.2, by applying the methodology described in Section 5.3.

The aircraft noise simulation framework was already subjected to preliminary testing for future research. Aurelization of the simulated noise was the first test done and yielded some interesting results which are shown in Section 6.3.

6.1. Validation

To validate the noise simulations, three steps were taken. The first step was comparing the certification simulation of the refence aircraft to their real life counter parts. The noise levels of the reference aircraft were found in EASA's noise type certificate database [50]. This comparison is made in Subsection 6.1.1. The second step was comparing the results of the previous step to those obtained by Sahai [4]. This step is discussed in Subsection 6.1.2. By doing these two steps it is possible to assess the validity of the noise predictions and approve them for use in the analysis. The third and final step was comparing the shape of the noise contours, which is done in Subsection 6.1.3. An additional step was done in which the noise performance of the reference and Initiator aircraft were compared. The results of this are shown in Subsection 6.1.4. This comparison is made to assess the key difference between the reference and Initiator aircraft. However, it does not affect the analysis later on since the principles of noise work the same regardless of the aircraft used.

6.1.1. Noise Certification Results

The certification results of the simulated aircraft can be found in Table 6.1. The results are given for all three points: flyover, lateral, and approach. For the reference aircraft the real life certification values from EASA are given as well. Since the Initiator aircraft do not have real life counterparts they cannot be compared and are thus not used in this validation step.

Table 6.1: Validation of aircraft noise certification results

Aircraft	*A320 ref.*	*A320 Ini.*	*A330 ref.*	*A330 Ini*	*F100 ref.*	*F100 Ini.*	*LR 1 ref.*	*LR 1 Ini.*	*LR 2 ref.*	*LR 2 Ini.*
MTOW [t]	71.5	71.7	242.0	244.9	44.5	44.5	181.4	228.4	351.5	426.8
W. Area [m^2]	122.4	112.1	361.3	412.4	93.5	105.7	283.3	383.6	436.8	623.5
W. Span [m]	33.9	32.42	58	61.8	28.1	29.9	47.6	55.4	73.9	73.6
Length [m]	37.6	35.8	62.45	64.8	32.5	32.2342	53.7	50.4	73.9	67.8
Thrust [kN]	2x117.9	2x117.9	2x297.44	2x297.44	2x67.2	2x67.2	2x267.03	2x267.03	2x513.9	2x513.9
BPR [-]	5.9	5.9	5.1	5.1	3	3	5.1	5.1	7.08	7.08
T/W	3.30	3.29	2.46	2.43	3.02	3.05	2.94	2.34	2.92	2.41
W/S	584.15	639.52	669.80	593.85	475.94	421.04	640.44	595.28	804.80	684.50
Certification INSTANT [EPNdB]										
LAT	88.1	88.2	89.0	89.0	87.8	88.2	89.6	88.4	92.2	92.6
TKO	91.7	94.1	98.4	98.4	89.7	89.1	94.4	99.2	102.3	106.2
APP	96.7	99.7	100.2	100.2	96.3	95.4	98.2	100.9	110.6	109.7
LAT+TKO	179.8	182.3	187.4	187.4	177.5	177.2	184.0	187.6	194.5	198.7
Cum.	276.5	281.9	287.5	287.6	273.7	272.6	282.1	288.4	305.0	308.4
Certification EASA [EPNdB]										
LAT	93.2	N/A	98.8	N/A	91.7	N/A	95.8	N/A	98.7	N/A
TKO	82.7	N/A	93.6	N/A	81.8	N/A	90.7	N/A	92.8	N/A
APP	94.2	N/A	99.5	N/A	93	N/A	97.5	N/A	100.5	N/A
LAT+TKO]	175.9	N/A	192.4	N/A	173.5	N/A	186.5	N/A	191.5	N/A
Cum.	270.1	N/A	291.9	N/A	266.5	N/A	284	N/A	292	N/A
Difference [EPNdB]										
LAT	-5.1	N/A	-9.8	N/A	-3.9	N/A	-6.2	N/A	-6.5	N/A
TKO	9.0	N/A	4.8	N/A	7.9	N/A	3.7	N/A	9.5	N/A
APP	2.5	N/A	0.7	N/A	3.3	N/A	0.7	N/A	10.1	N/A
LAT+TKO	3.9	N/A	-5.0	N/A	4.0	N/A	-2.5	N/A	3.0	N/A
Cum.	6.4	N/A	-4.4	N/A	7.2	N/A	-1.9	N/A	13.0	N/A

The results shown in Table 6.1 have also been condensed in Figures 6.1a and 6.1b. In these figures the simulated certification noise level is plotted against the actual certification levels. In general it can be seen that the flyover noise is 5 to 10 EPNdB above the levels recorded by EASA. A similar pattern can be spotted for approach, albeit with a smaller difference of around 2 EPNdB. The long range aircraft 1 is an exception to this with a difference of 10 EPNdB, i.e. nearly equivalent to the difference at flyover. For this aircraft, the overprediction is due to the GE90 engine, which has a considerably large bypass ration. Heidmann's fan model has problems predicting this fan noise for this engine size, resulting in the difference. For the sideline noise a difference between 3 to 10 EPNdB can be seen, as the lateral noise is underestimated. The sum of flyover and lateral noise represents a measure for the noise during take-off. Here it can be seen that the noise is in general overestimated by at least 3 EPNdB, with the A330 and long range aircraft 1 as exceptions. For the cumulative noise level of all three points, a similar observation can be made.

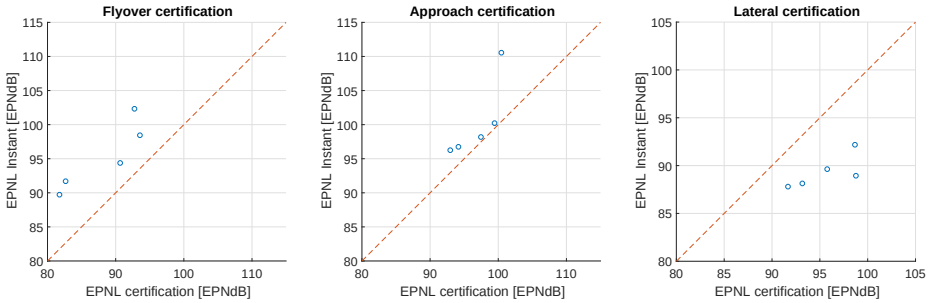

(a) The certification values at the three measurement locations

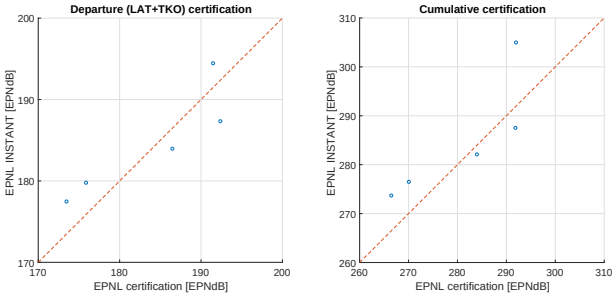

(b) The cumulative certification values

Figure 6.1: Validation of the simulated certification values

Aircraft manufacturers use trajectories which are highly optimised for noise. However, as explained in Section 5.2, this project uses trajectories resembling day to day operations. Therefore, the results in Table 6.1 and Figure 6.1 should not be used to dismiss the results of this project.

6.1.2. Comparison to Previous Research

The difference in trajectories can be a valid explanation for the offset in certification noise. To be certain, the found difference has to be compared to those found by Sahai [4]. Table 6.2 gives the margin between certification noise simulated by INSTANT and the noise registered in the EASA database, for a short range aircraft.

Table 6.2: Comparison of results to previous research

	TUDelft	Sahai [4]
LAT [EPNdB]	-5.1	+2.3
TKO [EPNdB]	+8.9	+3.3
APP [EPNdB]	+2	+4.7

From Table 6.2 it is clear that the margin to reality for this thesis is larger than earlier research. The main reason for this was found to be the aircraft's trajectory, as illustrated in Figure 6.2. The trajectory of Sahai was found using the Mikado design tool, which resulted in a trajectory which is higher during the initial stages of flight. At the flyover certification point Sahai's aircraft is at an altitude of approximately 1000 m, while the Initiator aircraft is at 600 m. As a result the noise emitted by the aircraft from this project experiences less attenuation effects. For geometric spreading alone the difference between the two aircraft is 4.4 dB. From this example it is clear that the difference between the margins found by the two research projects are nearly entirely due to trajectories.

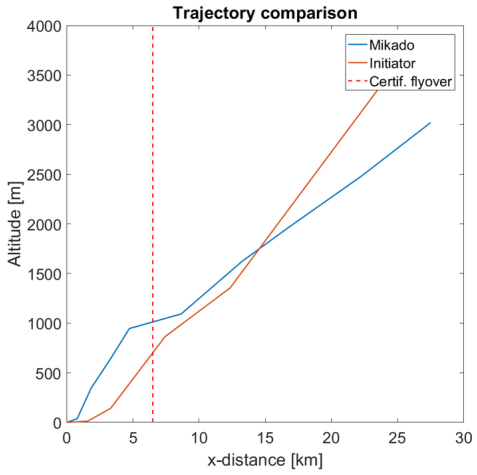

Figure 6.2: Comparison of the trajectory of a short range aircraft

6.1.3. Noise Contour Shape

The raw numbers at the three certification points seem reasonable. However, noise extends beyond these three points. To judge whether the simulations are representative, one should look at the shape of the noise contours. The EPNL, SPL, and SEL departure contours for the reference version of the Fokker 100 can be found in Figure 6.3.

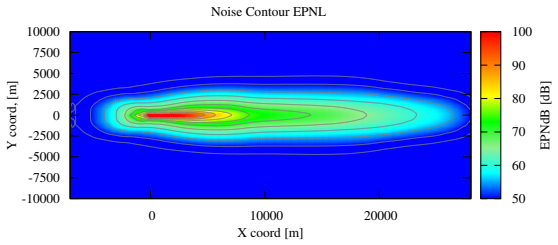

(a) The EPNL departure contour for the reference F100

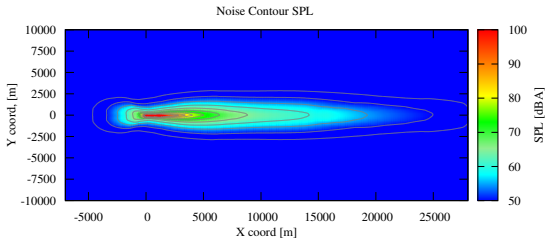

(b) The SPL departure contour for the reference F100

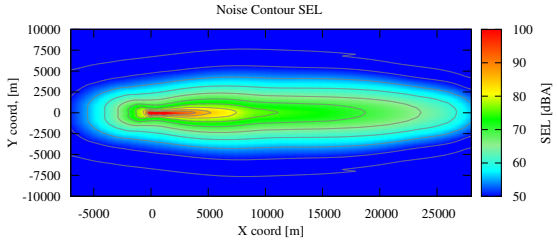

(c) The SEL departure contour for the reference F100

Figure 6.3: The three noise contours for the reference Fokker 100

The shape of the contours in Figure 6.3 seems reasonable when compared to references such as [4] and [51]. The same can be said about the EPNL, SPL, and SEL contours during approach for the Fokker 100. The three approach contours are shown in Figure 6.4:

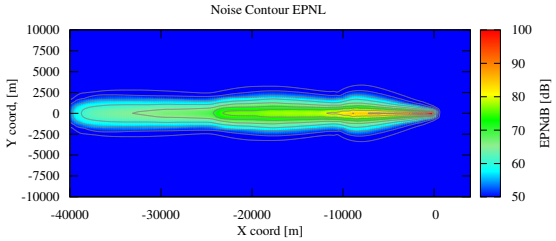

(a) The EPNL departure contour for the reference F100

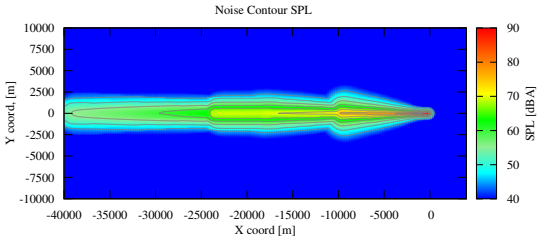

(b) The SPL departure contour for the reference F100

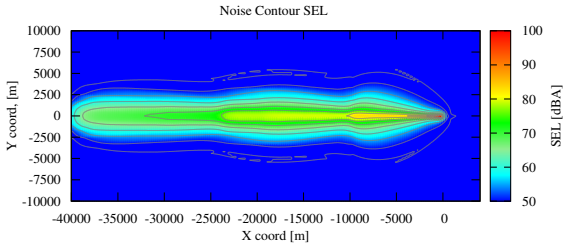

(c) The SEL departure contour for the reference F100

Figure 6.4: The three noise contours for the reference Fokker 100

The departure and approach contours for the remaining aircraft showed the same trends in shape as the contours shown in Figures 6.3 and 6.4. These trends are caused by the flight procedures and the scheduling of flap, slat and landing gear deployment. This is illustrated by Figures 6.5a and 6.5b, where the scheduling is compared to the SPL contours.

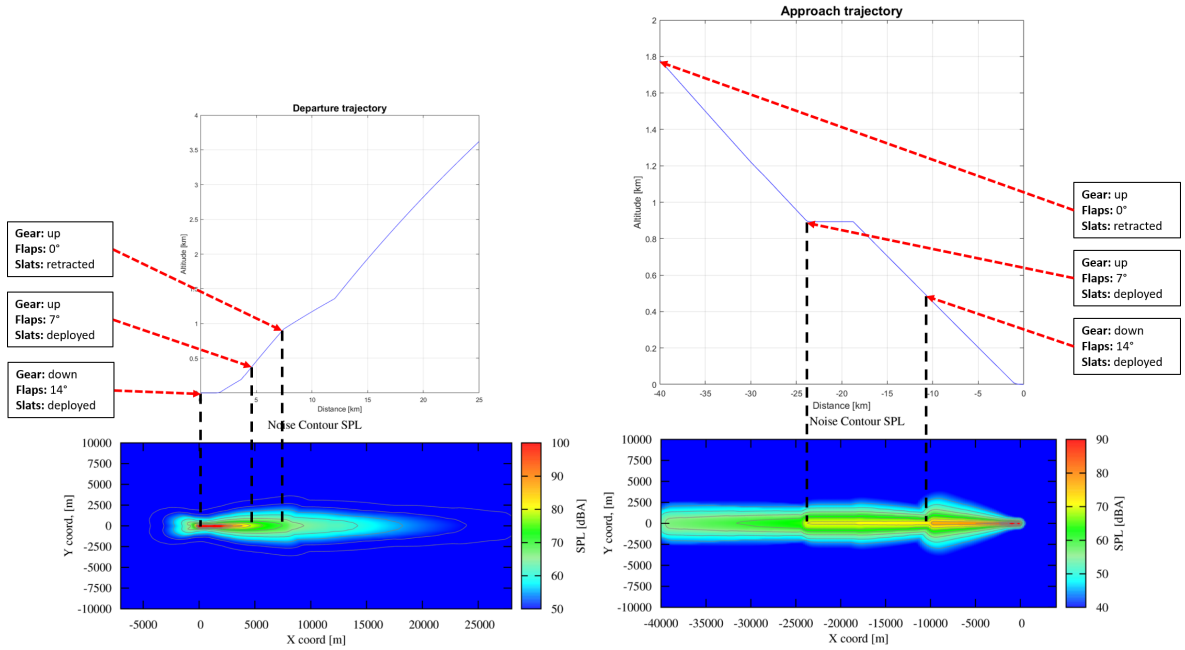

(a) Consequences of the flight procedures on the departure SPL contour

(b) Consequences of the flight procedures on the approach SPL contour

Figure 6.5: The effects of flight procedures on the noise contours

The effects shown in Figure 6.5 are mainly noticeable during approach. During departure these effects are more subtle. This is because the shape of the departure contour is mainly defined by the NADP1 procedure.

For approach, it can clearly be seen, through the widening of the contour, that the deployment of the flaps and slats increases the noise around 24 km from the runway. After the level flight part between 24 and glideslope interception at 19 km, the aircraft starts descending again and the contour becomes more narrow. That is, until further deflection of the flaps and the deployment of the landing gear, approximately 10 km from the runway. These effects are seen in the noise contours of all ten aircraft for each of the three metrics. As previously mentioned, the flap, slat and gear deployment scheduling is hard coded into INSTANT. Therefore, all aircraft have the same degree of flap deployment. In reality, each aircraft has varying degrees of deflection. For future work it is advised that flap, slat, and gear deployment are determined in the trajectory model and passed to INSTANT within the XML trajectory files.

This section showed that the simulated noise results are within reasonable bounds. Hence, they are reflective of reality even though they might overestimate the noise produced by the aircraft. As a result these simulations can be used in the investigation of the relationships between EPNL, L_A, and SEL.

6.1.4. Comparison of Reference and Initiator Aircraft

Since the reference and Initiator version of the aircraft use the same engine model the differences in noise are due to trajectories and airframe geometry only. The effect of trajectories can be seen in Figure 6.6. For the A330 and F100, both the reference and Initiator versions have a nearly equal weight. As a result, the trajectory of the reference aircraft and the Initiator version almost coincide during departure, as seen in Figure 6.6a. This is then reflected into the certification noise results where both versions have near equal values at the flyover and sideline points. The opposite can be said for the long range aircraft 1 and 2. Initiator overestimated the weight of these aircraft, hence these versions fly lower than their real life counterparts. This is then again reflected in a higher measured noise level at the TKO and LAT points. For the approach all aircraft have nearly the same trajectory, since they are all at near idle thrust and follow the same glideslope angle. Hence, the differences measured at the APP point are purely due to a difference in airframe noise.

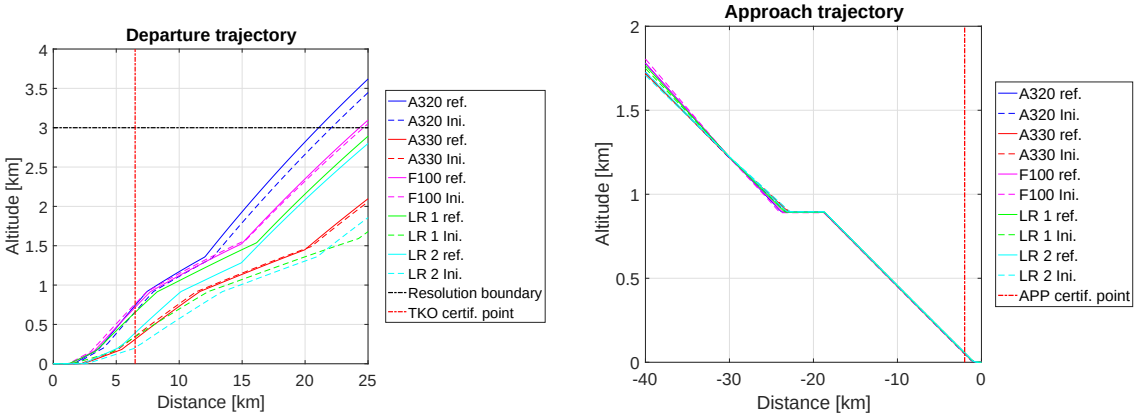

(a) The departure trajectories of the simulated aircraft

(b) The approach trajectories of the simulated aircraft

Figure 6.6: Comparison of the flight trajectories

The conclusion that the major difference in noise between the reference aircraft and the Initiator aircraft is due to airframe noise during approach. This is supported by the fact that airframe noise is the more dominant noise source during approach. This is shown in Figure 6.7b, where the noise measured at the approach certification point is broken down into separate components. The situation for departure is shown in Figure 6.7a, where it can be seen that engine noise is the more dominant noise driver. However since both versions use the same engine model the differences during departure originate from the trajectories. The aircraft at a higher altitude will experience more attenuation effects, hence it will be measured as being more silent.

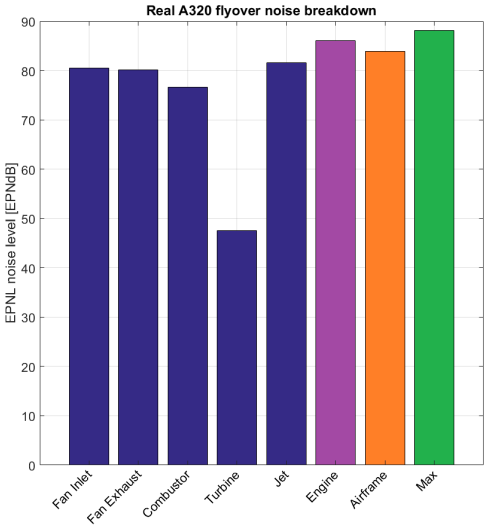

(a) Breakdown of the noise components measured by the flyover point

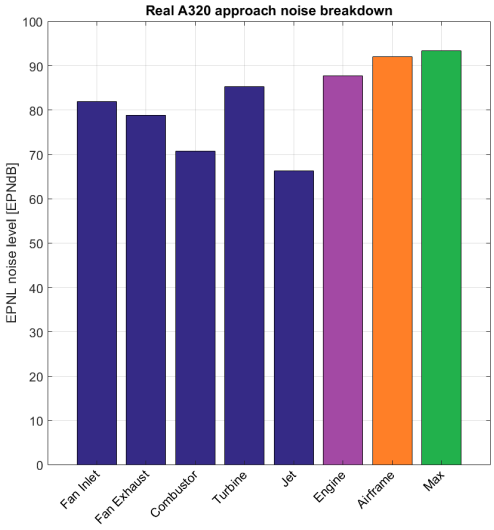

(b) Breakdown of the noise components measured by the approach point

Figure 6.7: Breakdown of the noise components for a simulated A320

6.2. Metric Relationship

In the previous section it was deemed that the simulation results are reflective to reality. Based on that, these results could be used for the investigation of noise metrics. While the previous section used only the reference aircraft, this Section will use both reference and Initiator aircraft. The reason for this is that validation required aircraft, which are exactly the same as those registered in the EASA noise certificate database. To investigate the relationship between metrics, it is not necessary to use real aircraft. As long as they behave as aircraft, the principles of noise apply.

The methodology for this investigation was explained in Section 5.3. The first step of was to compare the EPNL certification values with the areas within the noise contours. For this purpose the contours were defined at 65, 70, 75, 80, and 85 EPNdB or dB(A). For take-off the areas within the contours where compared to the summation of the EPNL levels at the flyover and lateral point. This was found to give better results than comparing just to flyover alone. For approach a first comparison was made with respect to the measurements at the approach point. However, this gave unsatisfactory results, hence the areas were compared to the cumulative level of the three measurement points. The results can be found in Figure 6.8, the R-squared values indicating the correlation can be found in the legends next to the plots.

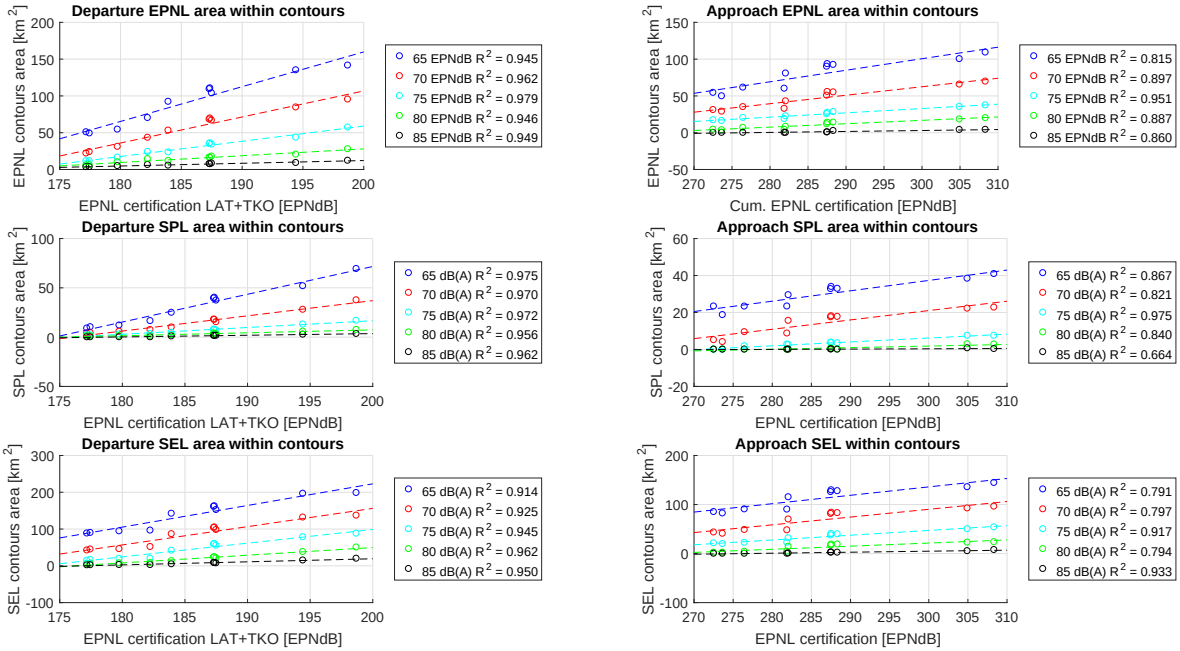

Figure 6.8: The relation between EPNL levels and areas within contours

Figure 6.8 shows a very strong relationship between the EPNL level of an aircraft and the area contained within the SPL, and SEL contours. Similarly, a linear relationship can be found between the SPL and SEL metrics. This indicates that a relationship exists between the EPNL level of an aircraft and the noise contours produced by this aircraft, even for different metrics. This also means that for a noise study, one could only investigate at the effects on EPNL and assume that the effects on SPL and SEL would be similar. This conclusion is also supported by the results of a NASA study, in which researchers used FAA's Integrated Noise Model, INM, to investigate the relationship between EPNL and SEL. This study also found a strong linear regression between EPNL and SEL, while looking at a much larger dataset [51]. It should be noted that these relationships are stronger for the departure than approach, a conclusion which is also found in the findings of NASA.

From the previous step, it is clear that a relationship exists between EPNL levels at certification point and the L_A and SEL contours. However, it was also investigated whether this holds true for the entirety of the contours. This was done by comparing the areas within the contours of EPNL, SPL, and SEL directly with each other. The results of this comparison can be seen in Figure 6.9.

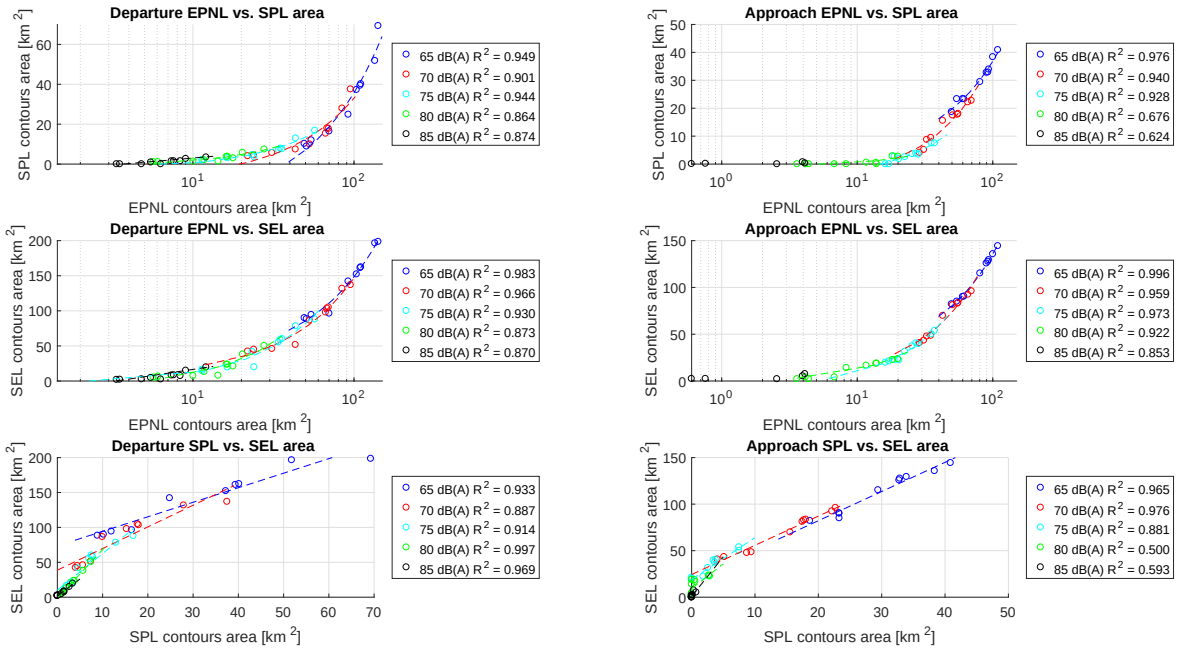

Figure 6.9: The relation between EPNL levels and areas within contours

Observing the correlations in Figure 6.9, it is clear that the relationships between the metrics exist on contour level as well. There is no directly noticeable difference between take-off and landing as both cases seem to have similar strong correlations. It can be seen though that the strength of this relationship diminishes for the higher decibel contours. Another interesting notion is that the relation between EPNL and SEL appears to be stronger than the one between EPNL and SPL. This might be due to both EPNL and SEL being time-integrated metrics.

The final step was relating the EPNL certification levels of the aircraft to the actual L_A and SEL levels at specified locations. This can be seen as constructing the L_A and SEL contours from the EPNL certification levels. Using traditional empirical methods it was tried to create a relationship with a form similar to Equations 6.1 and 6.2. However, despite trying several methods no relationship could be found suiting the ten aircraft.

$$L_{A_{x,y}} = f(EPNL_{A/C}, MTOW, b, S, l_{fuselage}, T, BPR, x, y) \tag{6.1}$$

$$SEL_{x,y} = f(EPNL_{A/C}, MTOW, b, S, l_{fuselage}, T, BPR, x, y) \tag{6.2}$$

For a while it seemed like this project had struck a roadblock. Until it was realised that in this day and age most calculations are done by computer. In the past, empirical relations were required to quantify and estimate intricate connections between several factors. This was done by weighting accuracy to computational effort. However, nowadays a computer can do that for you. It was decided to use a form of machine learning to solve this problem. Via the use of an *artificial neural network* (NN) the problem was finally solved. A neural network is a computational approach which is based on the structure of a biological brain. Similar to a real brain, a neural network consists of a collection of neural units (neurons) connected to each other by axons.

The network returns an output based on weighting functions present in each axon. Neural networks are capable of *learning*, in this case this means that given a specific task to solve, the network will use a set of observations to find the most optimal weighting to find the best fitting solution. The inputs for the neural network used in this project can be found in Table 6.3. The target which was used in the learning of this network were the EPNL, SPL, and SEL contours of the ten aircraft. The training data for this network were the results of the aircraft noise simulations done on the reference aircraft data set.

Table 6.3: Input for the neural network

Parameter	**Symbol**
MTOW [t]	W
Wing Area [m^2]	S
Wing Span [m]	b
Fuselage Length [m]	$l_{fuselage}$
Thrust [kN]	T
Bypass ratio [-]	BPR
Flyover level [EPNdB]	TKO
Lateral level [EPNdB]	LAT
Approach level [EPNdB]	APP
x location [m]	x
y location [m]	y

Note that two neural networks had to be created, one for departure contours and one for approach contours. The departure network uses all inputs from Table 6.3, except for the approach noise level. Similarly, the approach network does not use the flyover and lateral noise levels. It was also decided to limit neural network to the positive side of the y-axis. Doing so prevented the peak at the center line of the contour from being drastically reduced due to the fitting. The resulting network would then be mirrored to obtain the contour values for the negative y-values. Since the highest noise levels are found quite close to the runway (0-2 km), it was decided to split the contour, making a cut in the along the x-z plane at a y distance of 2 km. A network was created for the region below the 2 km line and another network for the region above the 2 km line. It was found that this method drastically improved the accuracy of the network close to the runway, having an R^2 value of approximately 0.98 for both departure and approach on the learning dataset. The result is a fast MATLAB function, which could be used to estimate the contours in programs where computational time is limited, such as Initiator. The neural network was then tested on the Initiator aircraft data set where it was shown to provide accurate results. An example can be seen in Figure 6.10. This figure shows the EPNL contour of the Initiator version of the A330 as simulated by INSTANT and as approximated by the neural network.

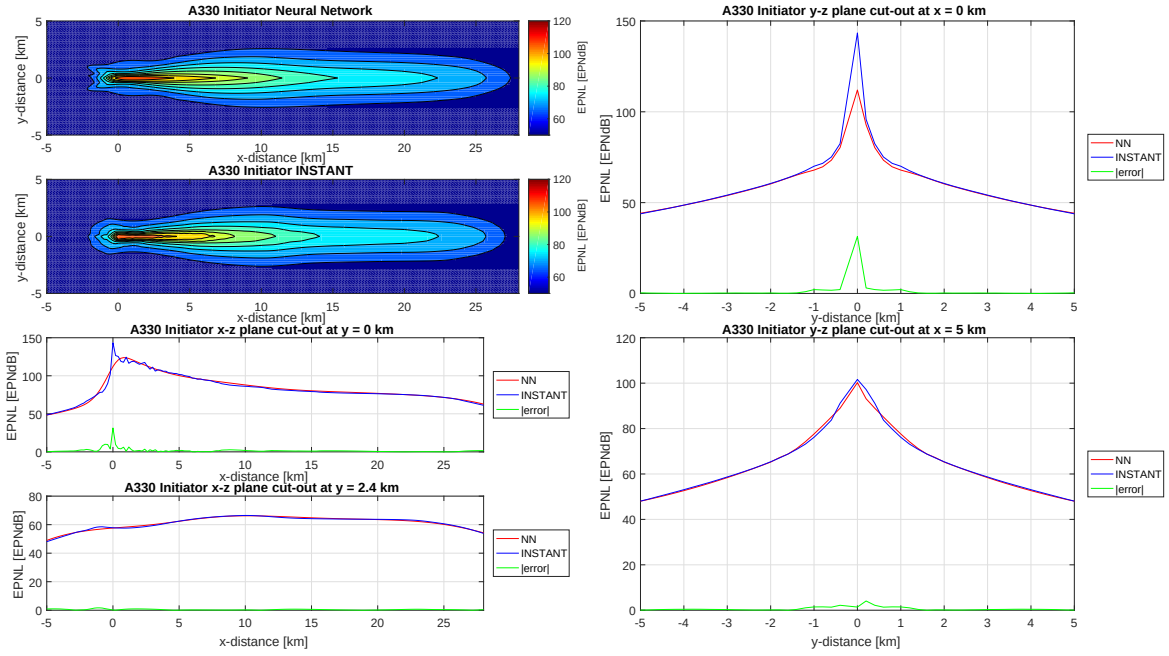

Figure 6.10: Comparison of the NN and INSTANT EPNL contour for an A330 departure

The general shape of the estimated contour is very similar to the contour created by INSTANT. When looking

at the cut-out plots it can also be seen that the magnitude of both contours is very similar. On overall the x-z plan cut-outs show a very good fit. The only region where the neural network makes some mistakes is near x = 0, y = 0. At this point the aircraft is at full throttle still on the runway. As a result this region has a very high peak noise level, which is smoothed out by the neural network as it needs to fit to the entire contour plot. At 5 km from the brake release point, the fit is much better. Looking at Figures 6.11 and 6.12 the same conclusions can be made.

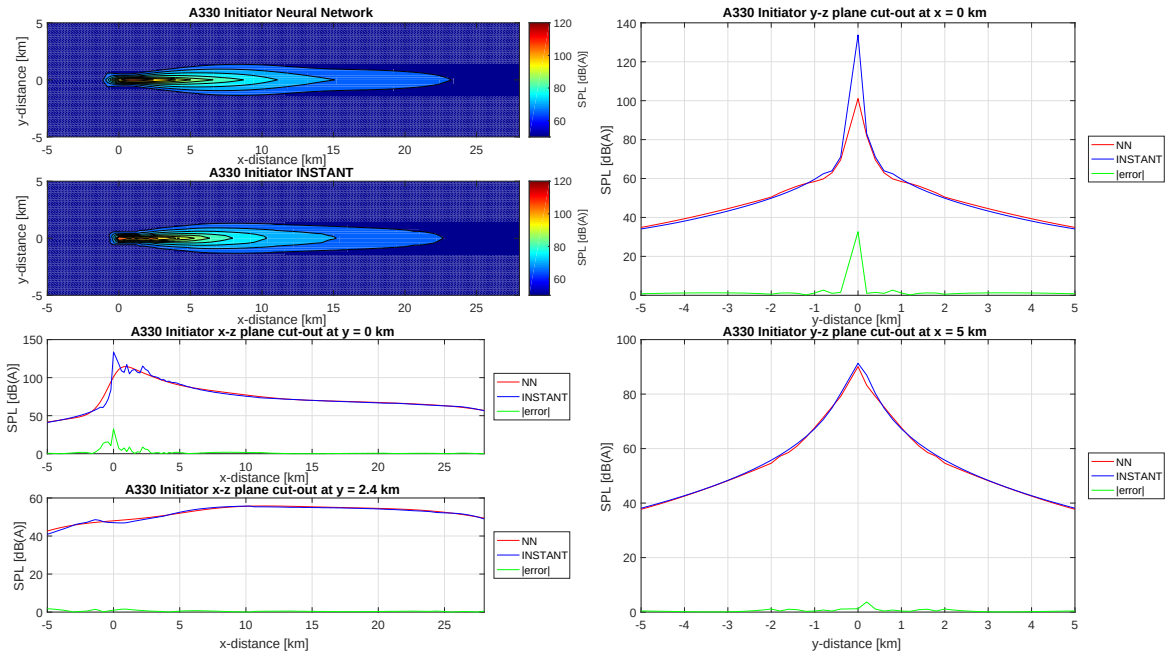

Figure 6.11: Comparison of the NN and INSTANT SPL contour for an A330 departure

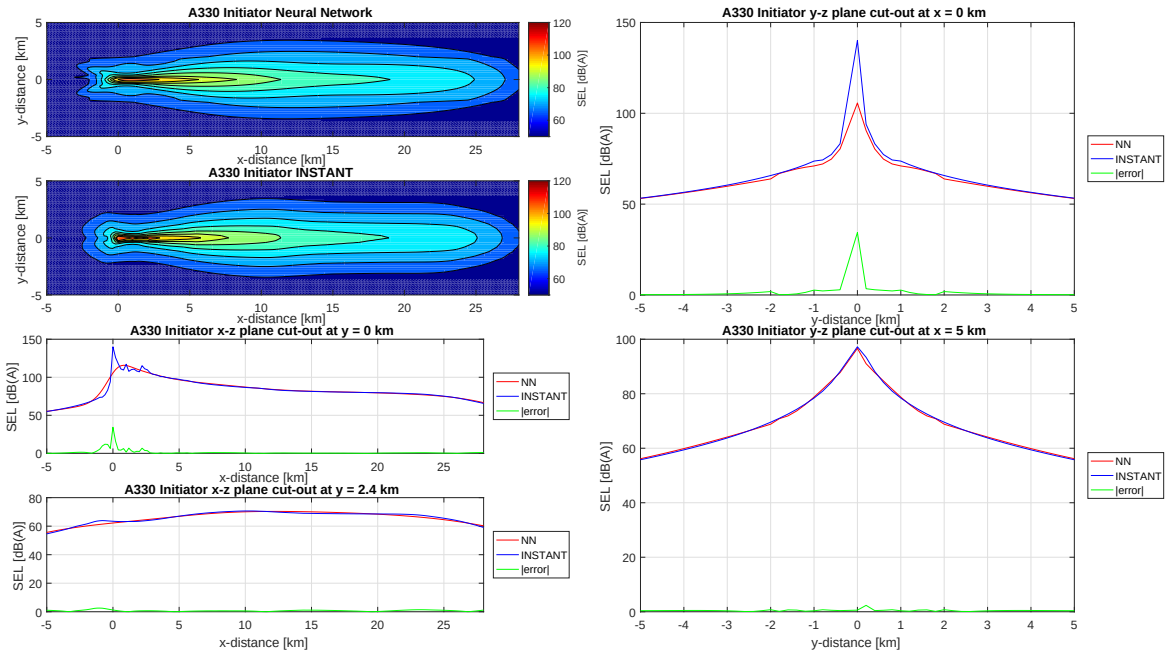

Figure 6.12: Comparison of the NN and INSTANT SEL contour for an A330 departure

The conclusions for departure are not entirely valid for approach as becomes clear in Figure 6.13. For approach, the shape of the contours lose their similarity, although the magnitude of the noise levels is still comparable. The magnitude also shows the same behaviour as for the departure contours, with the exception that the error margin becomes slightly larger in the lateral direction (as can be seen by the shape of the contours).

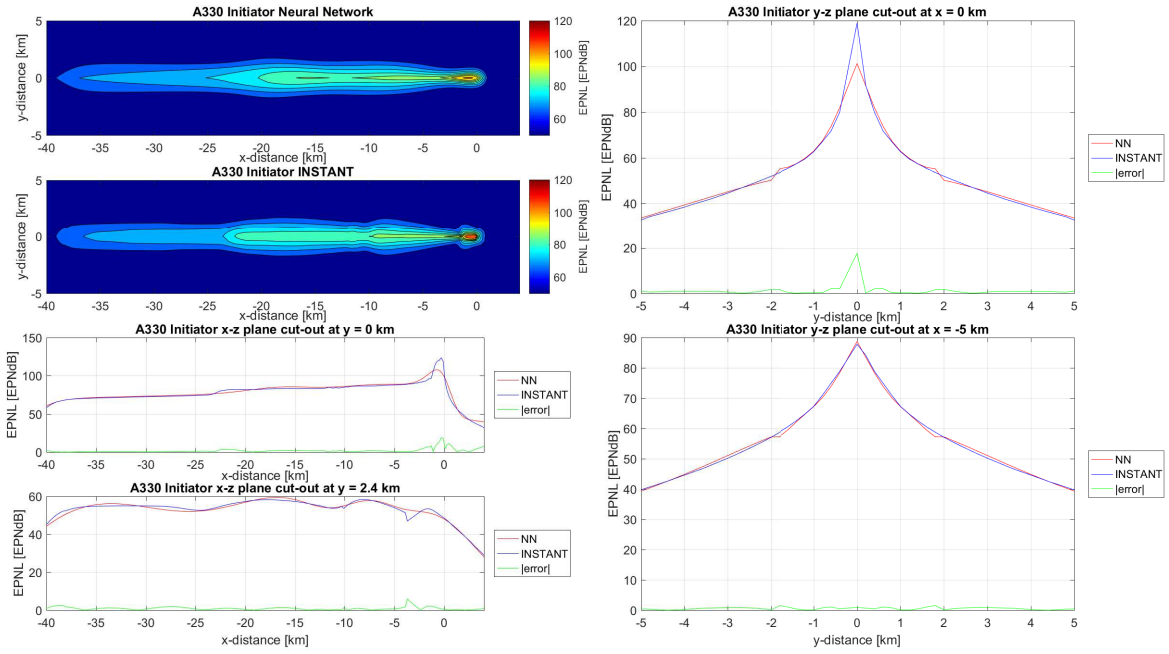

Figure 6.13: Comparison of the NN and INSTANT EPNL contour for an A330 approach

In Figures 6.10-6.12 it was seen that the neural network behaviour did not differ between the three metrics. The same conclusions were made for the approach phase, hence the plots for SPL and SEL during this stage are emitted for sake of conciseness. As could be seen in the approach plot, the shape of the neural network contours does not always match up nicely with the results from INSTANT. The conclusions regarding the departure and approach contours hold for the 9 other aircraft as well. This is illustrated by another validation mechanism in which the areas within the contours of the neural network were compared to INSTANT results. This is shown in Figure 6.14, where it is clear that there is an excellent match between the areas predicted by INSTANT and those estimated by the neural network.

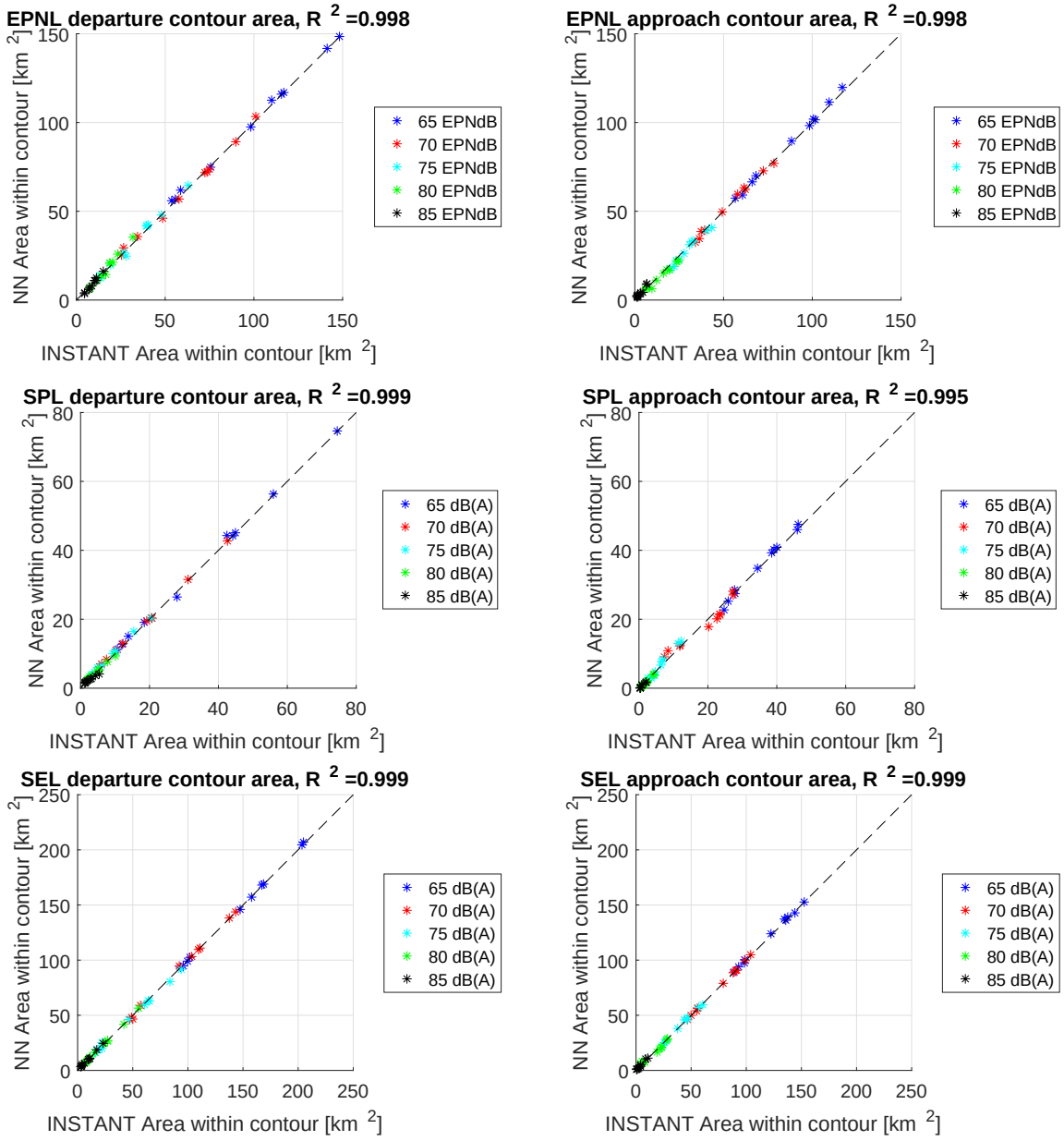

Figure 6.14: Comparison of the NN and INSTANT areas within contours

The neural network was also tested for aircraft with different geometries and noise values taken from the EASA database. It was found that the neural network behaved well with aircraft which were close to the training set. However, aircraft significantly smaller or larger than the learning set would result in inaccurate predictions.

It is expected that this problem can be remedied by expanding the learning dataset.

In conclusion it can be said that the neural network provides a solid relationship between the EPNL levels of an aircraft and the L_A and SEL levels. Although the general shape of the neural network contours might differ to those predicted by INSTANT it was seen that the difference in noise level was small. Additionally it was shown that the neural network is reliable at estimating the area contained within noise contours. Comparison with the areas enclosed within INSTANT generated contours yielded tiny differences. However, it turned out that the neural network does not behave well for aircraft which are significantly different than the learning set. To remedy this the learning set should be expanded with additional aircraft before this neural network can be used as an accurate prediction method.

6.3. Preliminary Results for Future Research

One of the intended uses of the aircraft noise simulation framework is the aurelization of aircraft noise. Aurelization is the technique in which the noise simulations are transformed into an audio file which can be played on a computer. The main advantage of this technique is that it makes noise simulations much more accessible to persons with no knowledge of acoustics. A secondary advantage is that the results from aurelization often show aspects of the noise not brought forward by decibel-metrics.

As an experiment,the approach of an A320 was simulated by the framework and aurelized. The aurelization exercise helped in identifying two issues:

1. The engine control input N1 was scheduled too smoothly in the trajectory model
2. The GSP model predicts a rather low temperature increase over the fan

To understand the first issue, let us take a look at Figure 6.15, which shows the variation of four parameters during the aircraft's approach. It can be seen that during the final moments of the approach, 20 km before the runway, the N1 spool speed continuously decreases until idle is reached. As a consequence, a continuous decrease is seen on the jet velocity along with a continuous narrowing of the noise contour as the aircraft descends, as seen in Figure 6.13. In reality, it would be impossible for a pilot to reduce N1 this slowly, unless aided by an autopilot. A more accurate reflection of N1 input is shown in Figure 6.16. Unfortunately, this was only observed at the end of the project, hence there was no opportunity to fully investigate the effects of this improved control input scheduling.

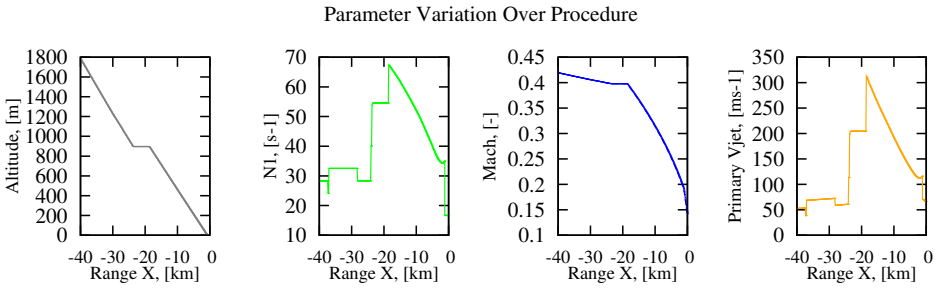

Figure 6.15: Current A320 parameter variation during approach

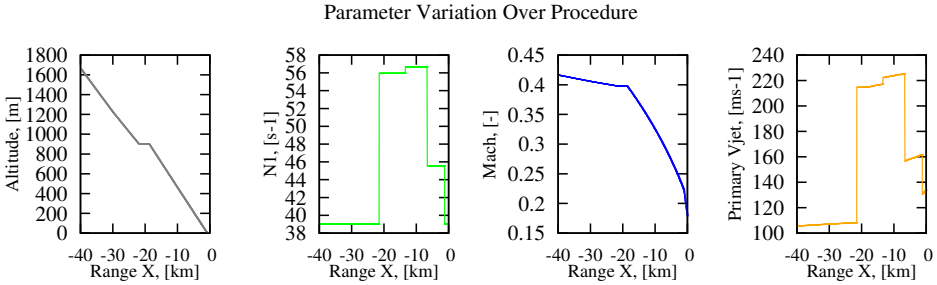

Figure 6.16: Improved A320 parameter variation during approach

It was also seen that the temperature rise across the fan was underestimated, averaging at a 3 K increase during near idle conditions for all engines. During aurelization this led to a lack of fundamental fan tones. The lack of fundamental tones can also clearly be seen in Figure 6.17a. A second simulation was made using an improved temperature rise across the fan resulting in stronger fan tones. These tones can clearly be identified in Figure 6.17b:

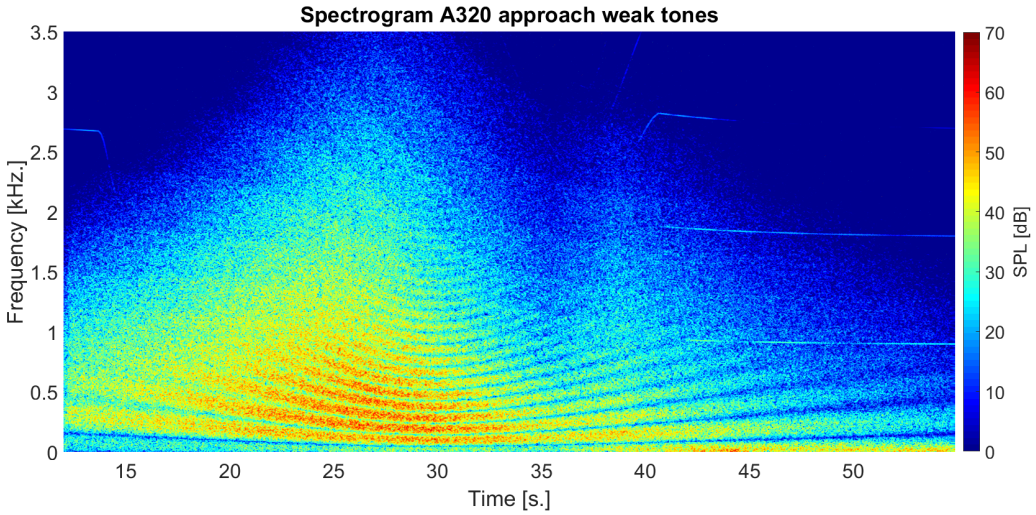

(a) Weak fan tones

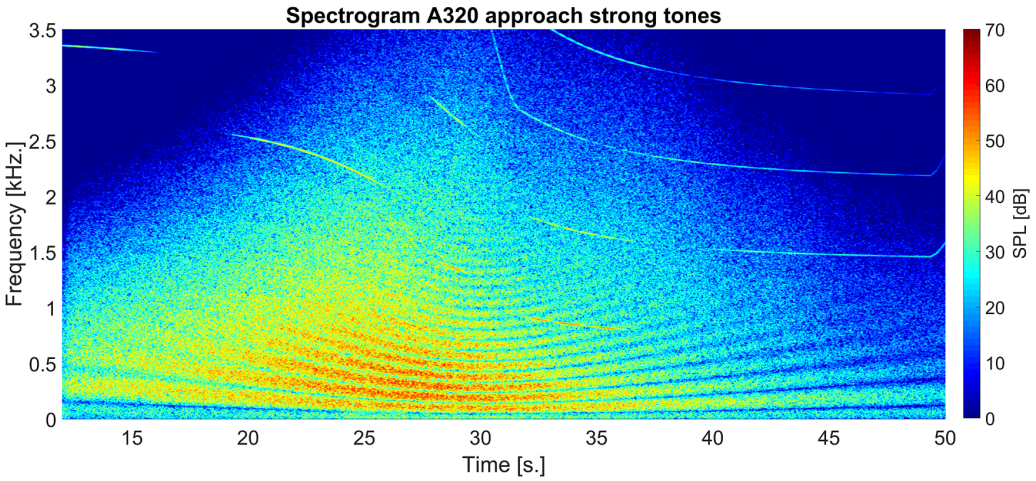

(b) Strong fan tones

Figure 6.17: Spectrogram of an A320 on approach as simulated by INSTANT

While both spectrograms in Figure 6.17 tell a different tale, the metrics do not. When looking at the L_A metric the weak tones flyover has a maximum SPL value of 68 dB(A), while the strong tones have an $L_{A,max}$ of 67 dB(A). For the SEL metric this is 77.5 and 77 dB(A), respectively. Since L_A is a frequency weighted metric this would indicate that both flyovers would be received as equivalent by the human ear. However, the strong fan tones flyover is perceived to be more annoying. This would have gone unnoticed in a classical analysis without aurelization and shows the advantages of this technique.

This chapter demonstrated the use of the aircraft noise simulation framework by analysing the relationship between the three metrics: EPNL, L_A, and SEL. It also provided a glimpse of the future research possibilities using this framework. Conclusions regarding these results and recommendations for improvement and future research are given in the next chapter.

7

Conclusion and Recommendations

The objective of this thesis was to investigate a relationship between aircraft noise levels given in EPNL and the noise levels given in L_A by creating an aircraft noise simulation framework. From Chapter 6 it can be concluded that this goal was met. The conclusions regarding this project can be found in Section 7.1. There are points of improvements for this research, but it also prepares the road for further investigations on aircraft noise. Recommendations regarding these improvements and future research can be found in Section 7.2.

7.1. Conclusions

The majority of the workload for this project went into the creation of the aircraft noise simulation framework. It was shown that with the models at hand within the FPP and ANCE departments, it is possible to give a good estimate of aircraft noise. To achieve this, the Intiator program was used to design aircraft, which were powered by engines modelled in GSP and flown by a point mass trajectory model. The results were used to estimate aircraft noise using the INSTANT noise prediction program.

Two types of aircraft were used: reference aircraft, which were geometrical one-by-one copies of actual aircraft, and Initiator aircraft which were made by Initiator based on the reference aircraft top level requirements. During validation only the reference aircraft were considered. These were validated by comparing to real life cases and examples in literature. For take-off and approach, it was seen that the aircraft noise certification values estimated by INSTANT were higher than those given by EASA, while the estimated sideline noise was lower. This can be explained by the fact that the flight procedures used are more reflective of day to day operations, whereas manufacturers use heavily optimised trajectories during certification. I.e. the flightpath of the aircraft in this project were lower than those during certification, as a result the emitted noise experiences less geometrical spreading and atmospheric absorption. Therefore, the measured noise during this project is higher than the values found in literature. This does not invalidate the results, and it is reckoned that steeper trajectories would result in smaller deviations. The noise contours generated by INSTANT are realistic as well, both in magnitude and shape. As a consequence, the noise simulation results could be used in the search for the acoustic relationship.

To establish a relationship between EPNL, L_A, and SEL, a three step process was applied:

1. The first step was to assess whether the EPNL noise level at the three certification points correlated to the areas within the three metrics' noise contours. For departure a very good linear correlation was found between the summation of the noise levels at the sideline and flyover point and the areas within the contours. On average, this correlation had an R^2-value of 0.955 for the three metrics. For approach, the relation was less well defined with an average R^2-value of 0.857, when the areas where compared to the cumulative EPNL level.
2. The second step was comparing the EPNL, L_A, and SEL areas to each other. It was observed that for both departure and approach a clear linear correlation exists between the three metrics.
3. Steps 1 and 2 indicated the existence of a relationship between the three metrics. The third and final step was to define this relationship.

Using traditional empirical methods, no relationship could be found where the aircraft EPNL certification values and other aircraft parameters related to the noise values of the three metrics. A solution was found in the form of artificial neural networks. This machine learning approach helped to define a relationship between the parameters shown in Table 7.1 and the noise levels of the aircraft for each of the three metrics at any x,y location.

Table 7.1: Input for the neural network

Parameter	**Symbol**
MTOW [t]	W
Wing Area [m^2]	S
Wing Span [m]	b
Fuselage Length [m]	$l_{fuselage}$
Thrust [kN]	T
Bypass ratio [-]	BPR
Flyover level [EPNdB]	TKO
Lateral level [EPNdB]	LAT
Approach level [EPNdB]	APP
x location [m]	x
y location [m]	y

The neural network was trained using the reference aircraft as training dataset and the Initiator aircraft as test case. The resulting network is a MATLAB function, which returns the noise levels at any given location of the contour with good accuracy for aircraft which are close to those of the training dataset. Noise contours generated by the neural network were compared to those simulated by INSTANT with respect to the area contained within the contours. It was found that the neural network gave a very good assessment of these areas, with only very limited differences to the areas predicted by INSTANT. Since this relationship is based on data of conventional aircraft, it is only applicable to standard wing fuselage configuration with two wing mounted engines. On the engine side, this relation is limited to two spool turbofan engines. Furthermore, it was seen that aircraft which were significantly smaller or larger than those of the training dataset provided inaccurate results. This behaviour can be improved by retraining the neural network with larger datasets. Taking these limitations into account, the function allows for the estimation of aircraft noise during the conceptual design stage with very limited input.

The scientific goal of this thesis was to find a relationship between EPNL, L_A, and SEL. It was found that these three metrics are clearly related. This means that during aircraft design one could look focus at one of these parameters and expect the other two to behave accordingly. A more complex relationship to estimate aircraft noise was found in the form of a neural network which can be used during the early stages of conceptual design. A secondary goal was the creation of the aircraft noise simulation framework. This was required to accomplish the main objective of this thesis and was accomplished using proven models available within the university. The results of the framework are reliable and deviations to reality and other research can be explained by the used flight trajectories. From the perspective of the Aircraft Noise & Climate Effects department, this framework offers many possibilities for future research.

7.2. Recommendations on Improvement and Further Research

Due to the scale of this project and the number of disciplines touched, there is a considerable amount of recommendations to be made. Most of these improvements will have a positive effect on the accuracy of noise predictions, while others will improve the general work flow of the framework. The improvements are:

- **Improvements to Initiator:**
  - Include a reliable high-lift-devices module: currently the effects of flap deployment on lift and drag are modelled as fixed increments.
  - Revise the landing gear sizing module: the current sizing module tends to generate unreasonable results for larger aircraft, such as an 11 meters long landing gear for the long range aircraft 2.
- **Improvements to the trajectory model:**
  - Reduction of computational time by the use of faster algorithms. Currently, the trajectory model is too slow for Initiator, taking roughly 3 to 5 minutes per calculated trajectory. Reducing this time would allow for the integration of the model into Initiator.
  - Implement a step-wise pilot input: the current input is continuous and adapted at each data point in the flight trajectory. A stepwise input would more accurately reflect pilot behaviour. This can be achieved by allowing control inputs to be changed once every x seconds rather than with each time step (as it is currently).
  - Improved model for high lift devices: currently the aerodynamics of high lift devices are only marginally accounted for in the trajectory model, due to the limited input from Initiator. It is also suggested to remove the hard coded flap and slat scheduling from INSTANT and use the flap and slat scheduling from the trajectory model instead.
  - Adaptation of the model to allow propeller aircraft: the flight performance and procedures for propellers are slightly different than those for jet aircraft. In order to estimate the noise from propeller aircraft, the trajectory model has to be adapted, this also applies to CROR powered aircraft. The main adaptions would be the introduction of control inputs such as the blade pitch angle.
  - Transition to a 3D model: the current model offers flight trajectories in 2D (x,z). A transition to a 3D model would allow the analysis of realistic flight procedures near airports. The adaptions required for this would be mainly to expand the equations of motion of the current trajectory model to include the third axis. However, this would be no easy task and building a new model from scratch might be more effective.
- **Improvements to GSP and engine models:**
  - Improve the iteration process of GSP: it was seen that, when calculating the engine decks, GSP would fail to converge after transitioning for near idle spool speeds to full throttle spool speeds.
  - Improve the engine models: aurelization showed that the engine models have some deficiencies such as the low temperature rise of the fan. Improvement of the models will improve the accuracy of the noise predictions.
- **Improvements to INSTANT:**
  - Follow up developments in noise modelling: follow up with the latest trends in the development of acoustic models and implement new models if these are beneficial.
  - Include additional noise models: to expend the capabilities of the aircraft noise simulation framework, more noise models should be included to INSTANT. Examples of models which can be included are: an engine shielding model such that fuselage mounted engines can be investigated and a CROR noise model.

  - Improve work flow: currently the input data for INSTANT is spread over 4 XML files: one simulation configuration file, one aircraft file, and two flight trajectories (one for departure and one for approach). The configuration file contains the simulation settings, but also the engine and aircraft geometry. The aircraft file contains the take-off thrust of the engine and the location and names of the trajectory files. The trajectory files contain the aircraft's position and engine thermodynamics. It is thus clear that the input for INSTANT is quite scattered and not always in a logical sense. To improve the work flow of the framework, the number of files could be reduced, for example by combining the general settings file with the aircraft file.

- **Improvements to the aircraft noise simulation framework:**

  - Work flow improvement: make sure that the compiler within the trajectory model directly generates all required input for INSTANT. This improvement should be made in parallel with the work flow improvement of INSTANT

Since this project combines the disciplines of the FPP and ANCE departments, it provides many interesting possibilities for future research. One interesting application is the aurelization of aircraft noise as has been shown in Section 6.3. The test case for aurelization showed that two noise measurements could have the same metric value for SPL and SEL, but can be very different in annoyance. This illustrates the need for further research into aurelization and psychoacoustics as the current noise metrics have their shortcomings. The framework could be used in this setting to investigate the drivers of aircraft noise by expressing it in actual sound rather than numbers. Another suggestion for future research is the implementation of aircraft noise estimation into an MDO aircraft design loop, i.e. design for minimum noise impact. This design optimisation could even be combined with the emissions models in GSP, resulting in an aircraft design optimization process which takes the environment into account. The framework can also be used to investigate the effect of flight trajectories on the noise impact and research noise reducing techniques such as continuous descent trajectories. In overall, this thesis project has opened the doors to many future investigations over the years to come, which will contribute to a better understanding and modelling of aircraft noise.

Bibliography

[1] R. Girvin. Aircraft noise-abatement and mitigation strategies. *Journal of Air Transport Management*, 15(1):14–22, 2009.

[2] G.J.J. Ruijgrok. *Elements of Aviation Acoustics*. Delft University Press, 2004.

[3] M.J.T. Smith. *Aircraft Noise*. Cambridge University Press, 1989.

[4] A. Sahai. *Consideration of Aircraft Noise Annoyance during Conceptual Aircraft Design*. Phd thesis, Technischen Hochschule Aachen, 2015.

[5] N. Dickson. Aircraft noise technology and international noise standards. In *Action Plan on Emissions Reduction*. ICAO, 2014.

[6] Flight Operations Support & Line Assistance. Getting to grips with aircraft noise. Technical report, Airbus Customer Services, 2003.

[7] S. Hosder. *Clean wing airframe noise modeling for multidisciplinary design and optimization*. Phd thesis, Virginia Polytechnic Institute and State University, 2004.

[8] R.J.M. Elmendorp, R. Vos, and G. La Rocca. A conceptual design and analysis method for conventional and unconventional airplanes. In *ICAS 2014: Proceedings of the 29th Congress of the International Council of the Aeronautical Sciences, St. Petersburg, Russia, 7-12 September 2014*. International Council of Aeronautical Sciences, 2014.

[9] L.L. Beranek. The noisy dawn of the jet age. *Sound and vibration*, 41(1):94–100, 2007.

[10] C. Lu and P. Morrel. Determination and applications of environmental costs at different sized airports – aircraft noise and engine emissions. *Transportation*, 33(1):45–61, 2006.

[11] Fraport AG. Airport charges at frankfurt airport. `http://www.fraport.com/content/fraport/en/misc/binaer/our-expertise/aviation-services/infographic--airport-charges-at-frankfurt-airport/jcr:content.file/fraport_entgelte_eng.pdf`. last accessed: 01/03/2017.

[12] Flughafen Munchen GmbH. Tariff regulations, part 1. `http://www.munich-airport.de/media/download/bereiche/aviation/charges2016.pdf`. last accessed: 01/03/2017.

[13] Flughafen Zürich AG. Airport charges at zurich airport. `https://www.zurich-airport.com/~/media/flughafenzh/dokumente/business_und_partner/flugbetrieb/20150301_gebuehrenreglement_en.pdf`. last accessed: 01/03/2017.

[14] Genève Aéroport. Airport charges and services. `https://www.gva.ch/en/Portaldata/1/Resources/fichiers/institutionnels/tarifs/tarifs_GVA_en.pdf`. last accessed: 01/03/2017.

[15] W. Dobrzynski. Almost 40 years of airframe noise research: what did we achieve? *Journal of Aircraft*, 47(2):353–367, 2010.

[16] ICAO Organisation. Icao annex 16, international standards and recommended practices. *Environmental Protection*, 2, 2008.

[17] K.D. Kryter and K.S. Pearsons. Judged noisiness of a band of random noise containing an audible pure tone. *The Journal of the Acoustical Society of America*, 38(1):106–112, 1965.

[18] Pratt & Whitney. Pratt & whitney pw1000g engine.
`http://www.purepowerengine.com`. last accessed: 01/03/2017.

[19] W.E. Zourmski. Aircraft noise prediction program theoretical manual. Technical Report TM 83199, NASA, 1982.

[20] M.R. Fink. Airframe noise prediction method. Technical Report FAA-RD-77-29, FAA, 1977.

[21] M.F. Heidmann. Interim prediction method for fan and compressor source noise. Technical Report TM-X-71763, NASA, 1979.

[22] J.J. Emmerling, S.B. Kazing, and R.K. Matta. Core engine noise control program. Technical Report FAA-RD-74-125, FAA, 1976.

[23] R.K. Matta, G.T. Sandusky, and V.L. Doyle. Ge core engine noise investigation - low emission engines. Technical Report FAA-RD-77-4, FAA, 1977.

[24] J.R. Stone. An improved prediction method for the noise generated in flight by circular jets. Technical Report TM-81470, NASA, 1980.

[25] K.B. Kontos, B.A. Janardan, and P.R. Gliebe. Improved nasa anopp noise prediction computer code for advanced subsonic propulsion systems. volume i: Anopp evaluation and nan noise model improvement. Technical Report CR-195480, NASA, 1996.

[26] K.B. Kontos, R.E. Kraft, and P.R. Gliebe. Improved nasa anopp noise prediction computer code for advanced subsonic propulsion systems. volume ii: Fan suppression model development. Technical Report CR-202309, NASA, 1996.

[27] J.H. Miles. Separating direct and indirect turbofan engine combustion noise while estimating post-combustion residence time using correlation function. Technical Report TM-2011-216248, NASA, 2010.

[28] C.K.W. Tam. Jet noise: since 1952. *Theoretical and Computational Fluid Dynamics*, (10):393–405, 1998.

[29] S.L. Heath and G.L. McAninch. Propagation effects of wind and temperature on acoustic ground contour levels. In *44th AIAA Aerospace Sciences Meeting and Exhibit*, Reno, Nevada, USA, 2006.

[30] L.C. Sutherland. Review of experimental data in support of a proposed new method for computing atmospheric absorption losses. Technical Report DOT-TST-75-87, US Department of Transport, 1975.

[31] American national standard method for the calculation of the absorption of sound by the atmosphere. Technical Report ANSI S1.26-1978, American National Standard Institute, 1978.

[32] C.F. Chien and W.W. Soroka. Sound propagation along an impedance plance. *Journal of Sound and Vibration*, 43(1):9–20, 1975.

[33] M.E. Delany and E.N. Bazley. Acoustical properties of fibrous absorbent materials. *Applied Acoustics*, 3(2):105–116, 1970.

[34] G. La Rocca, T.H.M. Langen, and Y.H.A. Brouwers. The design and engineering engine. Towards a modular system for collaborative aircraft design. In *28th International Congress of the Aeronautical Sciences*. International Council of the Aeronautical Sciences, 2012.

[35] J. van Dommelen and R. Vos. Conceptual design and analysis of blended-wing-body aircraft. *Proceedings of the Institution of Mechanical Engineers, Part G: Journal of Aerospace Engineering*, 228(13):2452–2474, 2014.

[36] E. Torenbeek. *Advanced aircraft design: Conceptual design, technology and optimization of subsonic civil airplanes*. John Wiley & Sons, 2013.

[37] D.P. Raymer. *Aircraft Design: A Conceptual Approach . Washington DC: American Institute of Aeronautics and Astronautics*. Inc, 1992.

[38] A. Elham, G. La Rocca, and M.J.L. Van Tooren. Development and implementation of an advanced, design-sensitive method for wing weight estimation. *Aerospace Science and Technology*, 29(1):100–113, 2013.

[39] K. Schmidt and R. Vos. A semi-analytical weight estimation method for oval fuselages in conventional and novel aircraft. In *52nd AIAA Aerospace Sciences Meeting*. American Institute of Aeronautics and Astronautics, 2014.

[40] M.F.M. Hoogreef. *The Oval Fuselage: A New Structural Design Concept for Blended Wing Body Cabins*. Phd thesis, TU Delft, Delft University of Technology, 2012.

[41] K. Tang, A.G. Rao, and J.P. van Buijtenen. Conceptual study of a hybrid turbofan engine with inter turbine burner. In *ASME Turbo Expo 2010: Power for Land, Sea, and Air*, pages 239–248. American Society of Mechanical Engineers, 2010.

[42] J.F. Sellers and C.J. Daniele. Dyngen: A program for calculating steady-state and transient performance of turbojet and turbofan engines. Technical Report TN-D-7901, NASA, 1975.

[43] W. Visser. *Generic analysis methods for gas turbine engine performance*. Phd thesis, Delft University of Technology, 2015.

[44] W.P. Visser, O. Kogenhop, and M. Oostveen. A generic approach for gas turbine adaptive modeling. *Journal of engineering for gas turbines and power*, 128(1):13–19, 2006.

[45] H. Cohen, G.F.C. Rogers, and H.I.H. Saravanamuttoo. *Gas turbine theory*. Longman Scientific & Technical Harlow (England), third edition, 1987.

[46] Anonimous. Iso 2533:1975 standard atmosphere. *International organization for standardization (ISO)*, 2533:1975, 1975.

[47] B.J. van Bruchem. *Fokker 100 Numerical Performance Model*. Master orientation project report, TU Delft, Delft University of Technology, 2015.

[48] FlightAscend Consultancy. Ascend fleets database. `http://www.ascendworldwide.com/what-we-do/ascend-data/aircraft-airline-data/ascend-online-fleets.html`. last accessed: 01/03/2017.

[49] European Aviation Safety Agency EASA. Icao aircraft engine emissions databank. `https://www.easa.europa.eu/document-library/icao-aircraft-engine-emissions-databank`. last accessed: 01/03/2017.

[50] European Aviation Safety Agency EASA. Easa approved noise levels. `https://www.easa.europa.eu/document-library/noise-type-certificates-approved-noise-levels`. last accessed: 01/03/2017.

[51] C.A. Powell. Relationship between aircraft noise contour area and noise levels at certification points. Technical Report TM-2003-212649, NASA, 2003.